HHS Public Access

Author manuscript

New Phytol. Author manuscript; available in PMC 2015 April 29.

Published in final edited form as:

New Phytol. 2014 September ; 203(4): 1175–1193. doi:10.1111/nph.12880.

Involvement of YODA and mitogen activated protein kinase 6 in Arabidopsis post-embryogenic root development through auxin up-regulation and cell division plane orientation

Veronika Smékalová[1,*], **Ivan Luptovčiak**[1,*], **George Komis**[1,*], **Olga Šamajová**[1], **Miroslav Ovečka**[1], **Anna Doskočilová**[1], **Tomáš Takáč**[1], **Pavol Vadovič**[1], **Ondřej Novák**[2], **Tibor Pechan**[3], **Anja Ziemann**[4], **Petra Košútová**[1], and **Jozef Šamaj**[1]

[1]Centre of the Region Haná for Biotechnological and Agricultural Research, Department of Cell Biology, Faculty of Science, Palacký University, Šlechtitelů 11, 783 71 Olomouc, Czech Republic

[2]Centre of the Region Haná for Biotechnological and Agricultural Research, Department of Metabolomics, Laboratory of Growth Regulators, Institute of Experimental Botany ASCR & Palacký University, Šlechtitelů 11, 783 71 Olomouc, Czech Republic

[3]Institute for Genomics, Biocomputing & Biotechnology, Mississippi State University, 2 Research Boulevard, Starkville, MS 39762, USA

[4]Institute of Cellular and Molecular Botany, University of Bonn, Kirschallee 1, 53115 Bonn, Germany

Summary

- The role of YODA MITOGEN ACTIVATED PROTEIN KINASE KINASE KINASE 4 (MAPKKK4) upstream of MITOGEN ACTIVATED PROTEIN KINASE 6 (MPK6) *was* studied during post-embryonic root development of *Arabidopsis thaliana*. Loss- and gain-of-function mutants of YODA (*yda1* and Δ*Nyda1*) were characterized in terms of root patterning, endogenous auxin content and global proteomes.
- We surveyed morphological and cellular phenotypes of *yda1* and Δ*Nyda1* mutants suggesting possible involvement of auxin. Endogenous indole-3-acetic acid (IAA) levels were up-regulated in both mutants. Proteomic analysis revealed up-regulation of auxin biosynthetic enzymes tryptophan synthase and nitrilases in these mutants. The expression, abundance and phosphorylation of MPK3, MPK6 and MICROTUBULE ASSOCIATED PROTEIN 65–1 (MAP65-1) were characterized by quantitative polymerase chain reaction (PCR) and western blot analyses and interactions between MAP65-1, microtubules and MPK6 were resolved by quantitative co-localization studies and co-immunoprecipitations.

Author for correspondence: Jozef Šamaj, Tel: +420 585634978, jozef.samaj@upol.cz.

*These authors contributed equally to this work.

Supporting Information

Additional supporting information may be found in the online version of this article.

- *yda1* and Δ*Nyda1* mutants showed disoriented cell divisions in primary and lateral roots, abortive cytokinesis, and differential subcellular localization of MPK6 and MAP65-1. They also showed deregulated expression of *TANGLED1 (TAN1)*, *PHRAGMOPLAST ORIENTING KINESIN 1 (POK1)*, and *GAMMA TUBULIN COMPLEX PROTEIN 4 (GCP4)*.
- The findings that MPK6 localized to preprophase bands (PPBs) and phragmoplasts while the *mpk6-4* mutant transformed with *MPK6AEF* (alanine (A)–glutamic acid (E)–phenylanine (F)) showed a root phenotype similar to that of *yda1* demonstrated that MPK6 is an important player downstream of YODA. These data indicate that YODA and MPK6 are involved in post-embryonic root development through an auxin-dependent mechanism regulating cell division and mitotic microtubule (PPB and phragmoplast) organization.

Keywords

Arabidopsis; cell division plane; MAP65-1; MAPKKK; microtubules; MPK6; root; YODA

Introduction

Asymmetric cell division and differential cell growth are both fundamental mechanisms underlying plant development and morphogenesis in the absence of cell motility (Rasmussen *et al.*, 2011a). Specific cell types (e.g. stomata; Lau & Bergmann, 2012) and entire organs (e.g. lateral roots; De Smet, 2012) originate from decisive asymmetric divisions, while specialized cell types such as Arabidopsis cotyledon and leaf pavement cells (Qian *et al.*, 2009) and trichomes and root hair cells (Tominaga-Wada *et al.*, 2011) are shaped by processes of spatially defined cell growth. In plants, cell division, cell growth and differentiation are affected by extracellular stimuli and intercellular interactions (reviewed in Rasmussen *et al.*, 2012).

Following such inputs, cell division may be symmetric or asymmetric, while the plane of cell division may lie transversely, longitudinally or obliquely to the cell axis (De Smet & Beeckman, 2011; Rasmussen *et al.*, 2011a). Auxin is the major plant hormone involved in the regulation of cell division, probably through activation of transcription factors such as AUXIN RESPONSE FACTORS (ARFs) and PLETHORA (Okushima *et al.*, 2005; Hofhuis *et al.*, 2013). Similarly, cell growth may be isotropic or anisotropic and diffuse or polar, yielding distinct cell types and guiding plant tissue and organ growth (Breuninger & Lenhard, 2010). All these morphogenetic processes are driven by proper, coordinated and conditioned organization of microtubules in the cell cortex (Szymanski & Cosgrove, 2009) and are consequently coupled to extracellular perception and its translation into cellular responses (Komis *et al.*, 2011).

From the mechanistic standpoint, the positioning of the cell division plane, the directionality of cell expansion and the patterns of cytomorphogenesis are determined by cortical microtubule arrays (Lloyd & Chan, 2008; van Damme, 2009). The cell division plane is marked by a cortical microtubule annulus accompanied or preceded by the respective

localization of microtubule-associated proteins (Buschmann *et al.*, 2006; Müller *et al.*, 2006; Walker *et al.*, 2007), signaling proteins (Xu *et al.*, 2008; Müller *et al.*, 2010; Komis *et al.*, 2011; Kirik *et al.*, 2012), endocytotic events (Dhonukshe *et al.*, 2005; Karahara *et al.*, 2009) and actin filaments (Panteris, 2008) called the preprophase microtubule band (PPB; Müller *et al.*, 2009).

The PPB marks quite accurately the future site of cell plate fusion to the parent walls by defining the plane of the centrifugal expansion of the cytokinetic phragmoplast (van Damme, 2009). However, the centrifugally expanding phragmoplast has a limited freedom of rotational motion out of the plane defined by the PPB, being continuously corrected by cortex–phragmoplast leading edge actin microfilament and microtubule attachments (Dhonukshe *et al.*, 2005; Higaki *et al.*, 2008).

In studies of microtubule-dependent mechanisms of plant cell division symmetry/asymmetry and cell growth directionality, mitogen-activated protein kinases (MAPKs) emerged as modal regulators (Beck *et al.*, 2010, 2011; Kosetsu *et al.*, 2010; Müller *et al.*, 2010; Komis *et al.*, 2011; Sasabe & Machida, 2012). In Arabidopsis, at least three Arabidopsis MAPKs, namely MPK4, MPK6 and MPK18, are implicated in microtubule organization and dynamics (Walia *et al.*, 2009; Beck *et al.*, 2010, 2011; Kosetsu *et al.*, 2010; Müller *et al.*, 2010). The developmental involvement of MPK4 occurs downstream of the Arabidopsis homologue of Nucleus and Phragmoplast localized kinase (ANP) family of MAPKKKs (Beck *et al.*, 2010; Kosetsu *et al.*, 2010) through the MAPKK MKK6 (Kosetsu *et al.*, 2010) and targets the MAP65-1, MAP65-2 and MAP65-3 microtubule-associated proteins, controlling their interaction with interphase and mitotic/cytokinetic microtubule arrays (Kosetsu *et al.*, 2010; Beck *et al.*, 2011; Sasabe *et al.*, 2011). Knockout mutants of any of the above constituents of the MPK4 pathway show incomplete cytokinesis and aberrant cytomorphogenesis as a result of disrupted phragmoplast progression and cortical array malorganization, respectively (Beck *et al.*, 2010, 2011; Kosetsu *et al.*, 2010).

MPK6, in contrast, seems to be involved in cell division plane determination as it interacts with the PPB and the phragmoplast, and co-fractionates and co-localizes with endocytotic markers. MPK6 depletion in *mpk6* mutants causes aberrant cell file formation in the root as a result of the disturbance of the cell division plane orientation (Müller *et al.*, 2010). MPK6 is directly phosphorylated by MKK4/5, which may be activated by alternative MAPKKKs including Mitogen-activated protein kinase kinase kinase 1 (MEKK1), ANPs and finally YODA (Colcombet & Hirt, 2008). YODA is a particularly interesting candidate in view of its developmental role in stomatal patterning. Two classes of mutants called *yda* (kinase inactive) and Δ*Nyda* (a gain of function), corresponding to the same MAPKKK4, have opposite effects on stomatal development, with *yda* plants showing clustering of stomata and Δ*Nyda* plants showing repression of stomatal development (Bergmann *et al.*, 2004; Wang *et al.*, 2007). Genetic disturbance of the components acting downstream of YODA, namely MKK4/5 and MPK3/6, leads to more exacerbated phenotypes, leading to the suggestion that stomatal development is strictly regulated by the YODA pathway (Wang *et al.*, 2007).

As a result of the connection of MPK3/6 with YODA signaling in the control of stomatal cell fate (Bergmann *et al.*, 2004; Wang *et al.*, 2007; Kim *et al.*, 2012), the embryonic

development (Lukowitz *et al.*, 2004) and the observation of similar developmental defects in primary roots of *mpk6* null mutants (Müller *et al.*, 2010), we focused here on root developmental phenotypes related to microtubule organization in allelic (loss-of-function) mutant of YODA (*yda1*; Lukowitz *et al.*, 2004) and in in-frame aminoterminal deletion mutant of YODA (Δ*Nyda1*; Lukowitz *et al.*, 2004), representing constitutively active form of MAP-KKK4. We also studied localization of MPK6 in living cells under control of a native promoter and phenotypes of *mpk6-4* mutants transformed with the kinase-dead form *MPK6AEF* (Bush & Krysan, 2007), which were very similar to *yda*.

Materials and Methods

Plant material and treatments

Sterilized seeds of *Arabidopsis thaliana* (L.) Heynh were imbibed and grown on Phytagel (Sigma, Prague, Czech Republic) solidified half-strength Murashige–Skoog (MS) medium, under axenic conditions as previously described (Beck *et al.*, 2010). All the seedlings used for further experimental processing were 3–14 d old. Two loss-of-function alleles of YODA (*yda*; At1g63700), namely the T-DNA insertional mutants *yda1* (which contains a stop codon within the catalytic kinase domain; Lukowitz *et al.*, 2004) and *yda2* (which is also kinase inactive with a proline substituted by a serine; Lukowitz *et al.*, 2004), two gain-of-function Δ*Nyda* alleles harboring aminoterminal deletions (Δ*Nyda1* and Δ*Nyda2*; Lukowitz *et al.*, 2004) and *mpk6-4* stably transformed with the *MPK6AEF* construct (Bush & Krysan, 2007), as well as the wild ecotypes Landsberg erecta (Ler) and Columbia (Col-0), were used throughout.

Three-day-old plants of Ler, *yda1* and Δ*Nyda1* growing on half-strength MS medium under standard growth conditions with dark-grown root systems were transferred to half-strength MS medium containing either 1 μM indole-3-acetic acid (IAA) or 10 μM auxinole (α-(2,4-dimethylphenylethyl-2-oxo)-IAA; auxin antagonist). Control plants were simultaneously transferred to basic half-strength MS medium. Subsequently, seedlings were cultivated under the same conditions for 5 d more. Primary root length and lateral root density were statistically evaluated using Student's *t*-test.

Root whole mount immunofluorescence localization of tubulin, MAPKs and MAP65-1

Root whole mount localizations of MPK3, MPK6, MAP65-1 and microtubules by indirect immunofluorescence were carried out exactly as previously described (Beck *et al.*, 2010) using the antibodies described in Supporting Information Methods S2. Fluorescently labeled samples (either Fei Mao (FM) 4–64 (FM 4–64), fixable FM 4–64 (FM 4–64 Fx) and 4′,6-diamidino-2-phenylindole (DAPI) stained roots or immunolabeled root whole mounts of Ler, *yda1* and Δ*Nyda1* seedlings) were examined with a Zeiss 710 CLSM platform mounted on a Zeiss Axio Imager Z.2 upright microscope (Carl Zeiss, Jena, Germany), using excitation lines at 405, 488 and 561 nm from argon, HeNe, diode and diode pumped solid-state lasers. Images were acquired with a dry 20×/NA 0.8, an oil immersion ×40/NA 1.40 or an oil immersion ×63/NA 1.46 objective, of which the latter two were corrected for coverslip thickness (no. 1.5/0.17 mm). Differential interference contrast images were acquired by filtering transmitted polarized light through a Wollaston prism. Samples were

examined by averaged eight-line scanning at a 16-bit color depth with a Nyquist-corrected planar resolution automatically set by Zeiss Zen 2012 software. Methods used for co-localization analyses are described in Supporting Information Methods S1.

Protein extraction, co-immunoprecipitation, Phos-Tag™ SDS-PAGE and western blot

Total protein extracts were obtained from the whole 14-d-old seedlings according to our previous work (Ovečka *et al.*, 2014). For western blot detection of phospho-MAPK species and correlation with MPK3 and MPK6, the same protein sample (Ler, *yda1* or Δ*Nyda1* extract) was loaded in three consecutive gel wells of either 8% Tris-Cl gels or 4–12% precast Tris-Cl gels (BioRad, Prague, Czech Republic). After transfer, polyvinyl difluoride (PVDF) membranes were stained with Ponceau S, allowing the visualization of the respective lanes. These were subsequently cut into strips and incubated with anti-pTEpY (anti-phospho-Threonine-Glutamic acid-phosphoTyrosine; Cell Signaling Technology, Biotech A.S., Prague, Czech Republic), anti-MPK3 or anti-MPK6 antibodies (Sigma-Aldrich). Chemiluminescence imaging of western blots was done with the ChemiDoc™ MP Imaging System (BioRad). Densitometric analyses of western blots were carried out with freeware IMAGEJ software (http://rsbweb.nih.gov/ij/).

For Phos-Tag™ (Wako Pure Chemical Industries Ltd, Osaka, Japan) phosphorylation analysis, radio-immunoprecipitation assay (RIPA) buffer (25 mM Tris-Cl, pH 7.4, 150 mM NaCl, 1mM ethylene glycol tetraacetic acid (EGTA), 1% v/v Nonidet P-40, 0.5% w/v sodium deoxycholate) was supplemented with 10 mM NaF and 100 μM Na_3VO_4, in order to avoid phosphate-containing phosphatase inhibitors that would interfere with the assay. For acrylamide-pendant Phos-Tag™ discrimination of phosphorylated from nonphosphorylated forms of the same protein, Phos-Tag™ and equimolar Zn^{2+} were co-polymerized with 7.5–10% Bis-Tris buffered sodium dodecyl sulfate–polyacrylamide gel electrophoresis (SDS-PAGE) gels (Fujita *et al.*, 2013). Proteins were resolved at 15–30 mA per gel in 100 mM 4-morpholinepropanesulfonic acid (MOPS), 100 mM Tris, 5 mM sodium bisulfite and 0.1% w/v SDS. Gels were washed with 10 mM ethylenediaminotetraacetic acid (EDTA) in Tris/glycine transfer buffer with 5% v/v methanol and subsequently in neat transfer buffer to remove Zn^{2+} cations before overnight wet transfer to PVDF membranes at 24 V.

For co-immunoprecipitation experiments, samples were processed exactly according to the instructions for the ChromoTek GFP-Trap®_A kit (Chromo Tek GmbH, Martinsried, Germany).

Cloning of MPK6 under a native promoter and transformation of *mpk6-2* mutants

Both the C-terminal and N-terminal fusions of GREEN FLUORESCENT PROTEIN (GFP) with AtMPK6 driven by its own promoter were prepared using genomic DNA from leaf tissue. The 1784-bp *AtMPK6* promoter upstream of the ATG start codon was amplified using respective primers Mpk6npF and Mpk6npR (Table S1). The *AtMPK6* genomic sequence for C-terminal fusion (GFP is fused with the C-terminus of MPK6) was amplified using primers Mpk6ctF and Mpk6ctR (Table S1) and the *AtMPK6* genomic sequence for N-terminal fusion was amplified using primers Mpk6ntF and Mpk6ntR (Table S1). The amplified promoter, *AtMPK6* genomic DNA and *enhanced GFP (eGFP)* were assembled

using a recombination reaction according to instructions included in the MultiSite Gateway® Three-Fragment Vector Construction Kit (Life Technologies Czech Republic s.r.o., Prague, Czech Republic) and cloned into pB7m34GW.0, which was then used for *Agrobacterium tumefaciens*-mediated floral dip transformation of Arabidopsis *mpk6-2*$^{-/-}$ mutant plants. Transgenic progeny was selected using 20 μM phosphinotricin or 250 mg l^{-1} BASTA®. Selected 5-d-old T2 plants were used for live imaging experiments. Localization of GFP-tagged MPK6 was determined with a Zeiss 710 CLSM platform or Lightsheet Z1 platform (Carl Zeiss, Jena, Germany). Roots were counterstained with FM4-64. Some images were post-acquisition processed using the Decon-volutionLab plugin (Biomedical Imaging Group, EPFL, Switzerland; http://bigwww.epfl.ch/) of IMAGEJ.

Measurements of endogenous auxin

Endogenous concentrations of free IAA and its catabolites/conjugates were determined using the LC-MS/MS (liquid chromatography–tandem mass spectrometry) method (Novak *et al.*, 2012). Briefly, 20 mg fresh weight of 14-d-old Arabidopsis seedlings of the control and mutant lines was collected, extracted in ice-cold 50 mM sodium phosphate buffer (pH 7) and purified by solid phase extraction (SPE) on hydrophilic-lipophilic balance reversed-phase sorbent columns (OasisR HLB; 1 cc/30 mg; Waters, Milford, MA, USA). To each extract, 5 pmol of [$^{13}C_6$]-IAA, [$^{13}C_6$]-oxIAA, [$^{13}C_6$]-IAAsp and [$^{13}C_6$]-IAGlu was added as internal standards to validate the quantification. Purified samples were analyzed using the LC-MS/MS system consisting of an ACQUITY UPLCR System (Waters) and XevoT TQ-S (Waters) triple quadrupole mass spectrometer. Quantification was obtained using a multiple reaction monitoring (MRM) mode of selected precursor ions and the appropriate product ion. For the Ler control and each mutant, four independent biological replicates were performed.

Chemicals, root morphometry and phenotyping, quantitative PCR and proteomic analyses are described in Methods S2–S6. All protein and peptide pertinent mass spectrometry data are available in Table S2.

Results

Root phenotypes of *yda* and Δ*Nyda* mutants

Previous studies showed that loss-or gain-of-function mutants of YODA affect stomatal fate as early as during the protodermal asymmetric definition of guard mother cell (GMC) precursors giving rise to GMCs (Bergmann *et al.*, 2004). However, *yda* mutants show also defects in embryonic and seedling development, suggesting a general role of the YODA pathway in cell fate determination (Lukowitz *et al.*, 2004). As previously described, *yda* allelic mutants develop rosette leaves and shoot development is nearly abrogated (Lukowitz *et al.*, 2004). Δ*Nyda* mutants, in contrast, show severe defects in the aerial organs, including fusion of cotyledons (Lukowitz *et al.*, 2004). In both cases, the two loss-of-function alleles (*yda1* and *yda2*) and the two gain-of-function alleles (Δ*Nyda1* and Δ*Nyda2*) were similar in terms of plant phenotypes, and therefore *yda1* and Δ*Nyda1* were selected for detailed experiments. Cellular root phenotypes were evaluated exclusively in *yda1* and *mpk6-4* +

MPK6AEF mutants showing stomatal clusters as well as in Δ*Nyda1* mutants showing no stomata (Fig. S1).

An overview of *yda* and Δ*Nyda* seedlings showed obvious changes in root patterning and development when compared with the Ler wild-type (Fig. 1). Young 4-d-old seedlings of *yda* mutants showed short roots or in some exceptional cases no roots (Fig. 1b–d). Seedlings of Δ*Nyda* at this stage showed shorter, agravitropic and twisted roots (Fig. 1e,f). Differences in root patterning such as primary root lengths and lateral root density were still obvious (Fig. 1g–i) at later stages of root development (8 d after germination) as evidenced also by quantitative evaluation (Fig. 1j,k). Both *yda1* and Δ*Nyda1* mutants showed shorter primary roots and a higher density of lateral roots when compared with the Ler control (Fig. 1g–k). A similar trend was found in 14-d-old seedlings (Fig. S2).

Distances from root tips to the first visible root hair encompassing meristematic and early elongation zones were much shorter in mutant plants (Fig. S3). One possible explanation for such root phenotypes is termination of the primary root meristem and changes in the concentrations of endogenous auxin in these two mutants. Therefore, we compared endogenous concentrations of IAA in both mutants and Ler controls. Measurements showed significantly elevated IAA concentrations in both mutants as compared with the Ler control (Fig. 2a). At the tissue level, *yda1* showed a higher density of lateral root primordia and ectopic cell divisions in the pericycle (Fig. 2d), while Δ*Nyda1* showed ectopic cell divisions in the central cylinder and pericycle (Fig. 2f) but also vigorous twisting of all root tissues (Fig. 2g).

Because twisting is a typical feature of some microtubule-defective mutants (Furutani *et al.*, 2000; Sedbrook *et al.*, 2004; Ishida *et al.*, 2007; Buschmann *et al.*, 2009), the organization of cortical microtubules was studied in epidermal cells of the Δ*Nyda1* mutant and compared with that of the Ler control (Fig. 3). However, no significant differences in microtubule orientation and organization between the mutant and control were detected. The only visible difference was the formation of oblique cell walls between neighbor cells in the Δ*Nyda1* mutant (Fig. 3c). Oblique cell divisions were further studied and quantitatively evaluated after vital staining of roots with FM4-64 and by microtubule immunolabeling as described in the following sections in relation to auxin.

Root phenotypes of *yda1* and Δ*Nyda1* mutants after treatment with exogenous auxin and auxinole

We exogenously applied 1 μM IAA to the half-strength MS medium and observed the phenotypes of the mutant plants and Ler wild-types. Exogenously applied auxin reduced the length of the primary roots in Ler as well as in both mutants; however, differences between the auxin-treated wild-type and mutant seedlings were less pronounced than those between the wild-type and mutant seedlings in the absence of exogenous auxin (Fig. 4a–k). However, lateral root density after auxin treatment was similar in the control and in both mutants (Fig. 4l).

Next, we observed the effects of the auxin antagonist auxinole, which competes with auxin for binding sites on the auxin receptor TRANSPORT INHIBITOR RESPONSE 1 (TIR1).

Auxinole reduced primary root length in Ler but not in *yda1* and Δ*Nyda1* by comparison to mock treatment (Fig. 5a–j). The total number of lateral roots was lower in both mutants treated with auxinole (Fig. 5k). Interestingly, auxinole caused moderate twisting of control Ler roots and strong twisting of *yda1* roots, while twisting of Δ*Nyda1* roots was not significantly changed.

Proteomic analysis revealed up-regulation of auxin biosynthetic enzymes in *yda1* and Δ*Nyda1* mutants

To characterize the proteomes of Ler, *yda1* and Δ*Nyda1*, a shot-gun proteomic analysis was performed employing two-dimensional nano-LC-MS/MS. Identification and quantification details for differentially abundant proteins identified in *yda1* and Δ*Nyda1* are provided in Tables S3 and S4.

The comparative analysis detected 92 up-regulated proteins (with at least 1.5-fold increased abundance) and 10 unique proteins in the *yda1* mutant. In contrast, 20 proteins were less abundant and an additional seven proteins were not detected in the *yda1* mutant. The same analysis of Δ*Nyda1* resulted in 52 up-regulated and 23 Δ*Nyda1* unique proteins, as well as 15 down-regulated and 18 wild-type unique proteins.

The classification of differentially regulated proteins using Kyoto Encyclopedia of Genes and Genomes (KEGG) annotations generated by the Search Tool for the Retrieval of Interacting Genes/Proteins (STRING) web-based application (Jensen *et al.*, 2009) is presented in Figures S4–S6.

Notably, several proteins involved in auxin biosynthesis were up-regulated in both mutants. Tryptophan synthase alpha chain, an enzyme involved in the synthesis of the auxin (IAA) precursor tryptophan, was detected in Δ*Nyda1* seedlings but not in Ler. Nitrilase 3 was identified as a unique protein in Δ*Nyda1*, while nitrilase 2 was identified as a unique protein in *yda1*. In addition, nitrilase 1 was 3.7-fold up-regulated in *yda1*. Nitrilases are enzymes that convert indole-3-acetonitrile to IAA in the indole-3-acet-aldoxime pathway (Bartel & Fink, 1994; Mashiguchi *et al.*, 2011).

Overall, these data indicate accelerated IAA synthesis in both the *yda1* and Δ*Nyda1* mutants, which exhibited higher concentrations of endogenous IAA. The increased levels of auxin biosynthetic enzymes help to explain the higher content of endogenous IAA in both mutants. This also suggests that the nitrilase pathway of auxin biosynthesis was probably up-regulated in the *yda1* and Δ*Nyda1* mutants.

Disturbance of cell division plane determination in *yda1* and Δ*Nyda1* mutants

The arrangement and patterning of cells and tissues in the *yda1* and Δ*Nyda1* mutants were surveyed in living roots by vital staining of cell membranes with the styryl dye FM4-64.

Cells in the root epidermis of Ler primary roots showed the normal succession from formative periclinal to proliferative anticlinal cell divisions, generating an ordered arrangement of cells into linear files (Fig. 6a,c). Also, the linear files of the inner root tissues

were well organized (i.e. the cortex, the endodermis and the pericycle). Quiescent central cells were typically shaped, ordered and surrounded by stem cell initials (Figs 6b,d, S7).

In *yda1* primary roots, the cell division patterns in the meristematic zone were disturbed. Many daughter cross-walls in epidermal and central confocal sections appeared oblique (Fig. 6e–h, m), while divisions of the meristem initials also appeared disordered (Figs 6h, S7). Similar root phenotypes and disturbances in cell division orientation were regularly recorded in *mpk6-4* mutants transformed with the kinase-dead form *MPK6AEF* (Bush & Krysan, 2007; Fig. S8). This suggests that MPK6 is a major player regulating cell division plane orientation downstream of YODA.

Finally, *c*. 7% of newly divided root cells showed cytokinetic defects resulting in binucleate or multinucleate daughter cells with cell wall stubs (Fig. S9; 94 out of 1340 late cytokinetic or post-cytokinetic cells examined in total; *N = 37* roots).

In Δ*Nyda1* primary roots, cell division planes were also visibly affected in the root epidermis (Fig. 6i,k,m), the internal root tissues and the stem cell niche (Figs 6j,l, S7). In contrast to *yda1* primary roots, Δ*Nyda1* never exhibited incomplete cytokinesis and binucleate cells (60/60 late cytokinetic and 44/44 post-cyto-kinetic cells).

Subsequently, we examined cell arrangements in lateral roots of Ler, *yda1* and Δ*Nyda1* plants. In contrast to Ler lateral roots (Fig. 7a,b), those of *yda1* exhibited a severely distorted outline, due to the occurrence of bulged epidermal cells (Figs 7c,d,f, S9). Furthermore, many lateral root epidermal cells showed incomplete cytokinesis as evidenced by the observation of cell wall stubs (Fig. 7e). Incomplete cytokinesis in the case of *yda1* lateral roots was significantly more pronounced than in the primary root, as it affected nearly 17% of the total number of cells examined (159 cases out of 937 examined in total; *N* = 47 lateral roots).

In lateral roots of Δ*Nyda1* plants (Fig. 7g–j), cell division plane orientation was again affected, as was the case in primary roots in both epidermal and internal root tissues (Fig. 6i–l). In contrast to *yda1* lateral roots, however, incomplete cytokinesis was never observed.

Visualization of mitotic and cytokinetic microtubule arrays in the root meristem of *yda1* and Δ*Nyda1* mutants

Cell division plane determination (which was presumably affected in *yda1* and Δ*Nyda1* primary and lateral roots) but also cytokinetic progression (which was probably affected in *yda1* lateral roots) are functions of specialized microtubule arrays such as the PPB and the phragmoplast. We therefore employed tubulin immunofluorescence labeling to follow microtubule organization in dividing cells of primary and lateral roots of *yda1* and Δ*Nyda1* plants, comparing it with the microtubule organization in Ler root cells (Fig. 8).

In Ler root cells, most PPBs and phragmoplasts were perpendicular to the root axis (Fig. 8a,d,g), with only a few being obliquely arranged (5% of PPBs (*N* = 23) and 7% of phragmop-lasts (*N* = 30)).

In primary and lateral roots of *yda1*, the numbers of oblique PPBs and phragmoplasts (Fig. 8b,e,h) were significantly increased (13% of PPBs (*N* = 22) and 51% of phragmoplasts (*N* =

35)) compared with Ler (Fig. 8a). Clusters of synchronously dividing cells were routinely observed (Figs 8b, S10). In Δ*Nyda1*, the percentages of oblique PPBs and phragmoplasts (Fig. 8f,i; 27% of PPBs (*N* = 35) and 59% of phragmoplasts (*N* = 59)) were substantially increased when compared with Ler. In addition, spindles were tilted in both mutants (Fig. 8b,c; 46% of spindles (*N* = 31)).

The cell division plane is controlled by several proteins including TAN1, POK1 and GCP4 (Müller *et al.*, 2006; Kong *et al.*, 2010; Rasmussen *et al.*, 2011b). Therefore, genes encoding these proteins were chosen for quantitative PCR analysis in both mutants and control plants. Results from qPCR analysis revealed that *TAN1* was more strongly expressed in *yda1* while it was less strongly expressed in Δ*Nyda1* (Fig. 8j). Also, *POK1* was less strongly expressed in Δ*Nyda1* while GCP4 was less strongly expressed in *yda1* (Fig. 8j). These expression changes in these genes might contribute to misaligned cell division planes in both mutants.

In *yda1* main roots, daughter cells with fully reconstituted nuclei able to organize radial perinuclear microtubules exhibited residual young phragmoplasts, suggesting a delay in phragmoplast expansion (Fig. 9a). This accounted for the majority of cytokinetic figures taken into account (24 out of 36 phragmoplasts from two different main and two lateral roots). In this respect, we also observed post-cytokinetic binucleate cells with incomplete daughter cell walls, suggesting a defect in cell plate formation during cytokinesis (Figs 9b–d, S9). In some instances, micronuclei were observed (e.g. Fig. 9c), probably arising from aberrant mitoses where individual chromosomes fail to congress with the rest (Fig. 9e).

Phosphorylation levels and abundance of MPK3 and MPK6 in *yda1* and Δ*Nyda1* mutants

The developmental roles of YODA involve signal transduction to MPK3 and MPK6 via MAPKKs such as MKK4, MKK5, MKK7 and MKK9 (Wang *et al.*, 2007). Here, we examined the abundance of MPK3 and MPK6 at the transcript and protein levels and the phosphorylation status of MPK3 and MPK6, as complete experimental data on the activity status of MPK3 and MPK6 are lacking in both mutants (Wang *et al.*, 2007).

First, we quantified transcripts of *MPK3* and *MPK6* in root extracts of Ler, yda1 and Δ*Nyda1* by real-time qPCR using the *ELONGATION FACTOR 1a (EF1a)* gene as a normalization standard. Transcripts of *MPK3* and *MPK6* were decreased in the *yda1* mutant (Fig. S11). By contrast, in the Δ*Nyda1* mutant *MPK3* transcripts were slightly but nonsignificantly increased, while *MPK6* transcript levels were similar to those of the Ler wild-type (Fig. S11). *YODA* transcripts were down-regulated in yda1 and strongly up-regulated in Δ*Nyda1* (Fig. S12), which confirms previously published results (Bergmann *et al.*, 2004).

At the protein level, MPK6 was more abundant than MPK3 in the roots of Ler (Fig. S13). Next, levels of phospho-MPK3 and phospho-MPK6 were investigated using a commercial anti-pTEpY antibody in comparison to specific anti-MPK3 and anti-MPK6 antibodies. Immunoblots revealed that levels of both phosphorylated MPK3 and MPK6 proteins were significantly increased in extracts of Δ*Nyda1*, but surprisingly they were also increased in extracts of *yda1* (Fig. 10a,c,d). The over-activation of MPK3 and MPK6 in *yda1* mutants

was also mentioned previously (Lampard *et al.*, 2009) but it has never before been demonstrated experimentally.

Partial co-localization of MPK6 and microtubules in root tip cells of *yda1* and Δ*Nyda1* mutants

The previous study showed that MPK6 partially co-localized with microtubule arrays and particularly with PPBs and phragmop-lasts (Müller *et al.*, 2010). Furthermore, the root phenotype described for *yda1* in the preceding sections showed a resemblance to the previously described root phenotypes of *mpk6* knockout mutants (Müller *et al.*, 2010). In the context of the possibly differential regulation of MPK6 in *yda1* and Δ*Nyda1* and the phenotypic similarities between *mpk6* and *yda* mutants, the subcellular localization of MPK6 in dividing cells of Ler, *yda1* and Δ*Nyda1* roots was investigated. MPK6 immunoreactive spots co-localized with both PPBs and phragmoplasts in root cells of Ler (Fig. 11a,b; 8/8 PPBs and 11/11 phragmoplasts from five roots in total). These spots were not exactly following the filamentous microtubule pattern within such arrays, but they were rather preferentially clustered in PPBs and phragmoplasts (Fig. 11a,b).

In *yda1*, both PPBs (Fig. 11c) and phragmoplasts (Fig. 11d) were consistently devoid of MPK6 immunostaining (17/17 PPBs from four roots and 33/33 phragmoplasts from 11 roots). Conversely, both PPBs (Fig. 11e) and phragmoplasts (Fig. 11f) were intensely labeled with anti-MPK6 antibody (18/18 phragmoplasts from seven roots and 9/9 PPBs from five roots) in the Δ*Nyda1* mutant.

Specific associations of GFP-tagged MPK6 with PPBs, phragmoplasts and cell plates (Fig. 12) were documented also in the *mpk6-2* mutant plants which were phenotypically rescued by *proMPK6::GFP:MPK6* and *proMPK6::MPK6:GFP* constructs (Fig. S14).

Western blot analyses with anti-pTEpY antibody showed that MPK3 was also robustly phosphorylated. Thus, as for MPK6, the probable differential localization of MPK3 in Ler, *yda1* and Δ*Nyda1* and its probable relationship to microtubule arrays were studied by co-immunolocalizations in root whole mounts. In all cases, the MPK3 signal exhibited a speckled cytoplasmic pattern but it was not related to microtubular structures such as PPBs and phragmoplasts (Fig. S15).

Differential distribution and altered co-localization of MAP65-1 and microtubules in *yda1* and Δ*Nyda1* mutants

Microtubule-associated protein MAP65-1 is a known target of MAPK signaling along with MAP65-2 and MAP65-3 (Beck *et al.*, 2010; Sasabe *et al.*, 2011) and it was identified as a target of MPK6 (Smertenko *et al.*, 2006; Popescu *et al.*, 2009; Hoehenwarter *et al.*, 2013). In this context, we next examined whether aberrant MPK6 signaling as a result of eliminated (*yda1*) or increased (Δ*Nyda1*) signaling by the YODA pathway would affect the subcellular localization of MAP65-1 in relation to the respective interphase and mitotic microtubule organization.

Furthermore, we quantified the co-localization of MAP65-1 with microtubules in cortical arrays, PPBs and phragmoplasts of Ler, *yda1* and Δ*Nyda1*. In this case, co-localization of

MAP65-1 with microtubules may be related to: the abundance of MAP65-1 protein (Mao *et al.*, 2005), and its affinity for the microtubule lattice as this is down-regulated by phosphorylation (Mao *et al.*, 2005; Smertenko *et al.*, 2006).

Immunofluorescent co-localization of MAP65-1 and microtubules in roots of Ler showed that MAP65-1 consistently co-localized with cortical interphase microtubule bundles, but also with PPBs and phragmoplasts in Ler (Figs 13a–c,j–l, S16–S18).

In *yda1* root cells, all the above-mentioned microtubule arrays were more strongly decorated with MAP65-1 (Fig. 13d–f). This was shown to be statistically significant when Pearson's coefficient for co-localization was taken into account (Figs 13j–l, S19–S21).

By contrast, cortical microtubules (Fig. 13g), PPBs (Fig. 13h) and phragmoplasts (Fig. 13i) of Δ*Nyda1* were nearly completely devoid of MAP65-1 as quantitatively demonstrated in co-localization analyses (Figs 13j–l, S22–S24).

Abundance and phosphorylation of MAP65-1 in *yda1* and Δ*Nyda1* mutants and interaction between MAP65-1 and MPK6

Quantitative fluorescence colocalization of MAP65-1 and microtubules showed increased amounts of microtubule-bound MAP65-1 in *yda1* and the near-depletion of microtubule-associated MAP65-1 in Δ*Nyda1*, probably owing to differential regulation of MPK6 in the respective mutants. This prompted us to examine whether MAP65-1 and MPK6 physically interact by means of co-immunoprecipitation. Results showed that MAP65-1 was pulled down, albeit quite weakly, with MPK6 in such co-immunoprecipitation assays (Fig. 13m), perhaps as expected for transient interactions of these two proteins (also mentioned in Popescu *et al.*, 2009). In Ler, *yda1* and Δ*Nyda1*, MAP65-1 total protein levels (tMAP65-1) analyzed by western blot were conserved against the alpha-tubulin loading control (Fig. 13n). The phosphorylated form of MAP65-1 (pMAP65-1) remained at moderate levels in Ler and *yda1* root extracts, but was significantly elevated in extracts from Δ*Nyda1* (Fig. 13n).

Discussion

Major phenotypic discrimination during stomatal ontogenesis shows that *yda1* mutants bear stomatal clusters while Δ*Nyda1* mutants form no stomata at all (Nadeau, 2009). Additionally, both mutants exhibit disturbed embryogenesis, which can be traced to the first asymmetric division of the zygote resulting in aberrant basal daughter cell formation (Lukowitz *et al.*, 2004). The embryonic YODA pathway seems to be triggered by the paternally inherited interleukin-1 receptor-associated kinase SHORT SUSPENSOR, which is N-myristoylated and S-palmitoylated, suggesting stable anchorage to the plasma membrane (Bayer *et al.*, 2009). Here, we experimentally investigated the orientations of cell divisions and cytokinesis in post-embryonic primary and lateral roots of *yda1* and Δ*Nyda1* mutants in relation to auxin. Genetic perturbation of YODA consistently affected cell division plane orientation and cytokinesis in the root meristems and affected primary and lateral root morphogenesis.

yda1 and Δ*Nyda1* mutants show auxin-related phenotypes

Phenotypic features of *yda1* and Δ*Nyda1*, such as shorter primary roots, a higher density of lateral roots and agravitropic and twisted growth of Δ*Nyda1*, suggested possible involvement of auxin (Tian *et al.*, 2004; Goh *et al.*, 2014). In addition, root twisting similar to that in Δ*Nyda1* was induced by auxinole, a TIR1 auxin receptor inhibitor (Hayashi *et al.*, 2008, 2012). Measurements of endogenous IAA showed a moderately increased concentration of IAA in the *yda1* mutant and a strongly up-regulated concentration of IAA in the Δ*Nyda1* mutant. Additionally, the Δ*Nyda1* mutant was at least partially insensitive to exogenously applied IAA. These findings were further strengthened by proteomic analysis, which revealed an overabundance of auxin biosynthetic enzymes such as tryptophan synthase and nitrilases in both mutants, which was again more pronounced in the Δ*Nyda1* mutant.

Previously it was reported that the auxin precursor tryptophan can induce more lateral roots (Dubrovsky *et al.*, 2008), which is consistent with the Δ*Nyda1* mutant showing up-regulated tryptophan synthase. At the subcellular level, auxin is the major regulator of cell division (De Smet & Beeckman, 2011), while cell division orientation and progression were significantly affected in both *yda1* and Δ*Nyda1* mutants.

Post-embryonic cell division defects in roots *of yda1* and Δ*Nyda1* mutants

It was suggested that YODA is somehow involved in asymmetric division in early embryo development (Lukowitz *et al.*, 2004) and that defects originating from loss of function may be carried over to future vegetative development. The proposed carryover may affect developmental aspects of root proliferation such as those including deregulated cell divisions in the stem cell niche. However, cytokinetic progression and cell division plane determination are general cellular mechanisms that are established in meristematic cells and are probably not embryo-specific. This is in accordance with the high expression levels of both MPK6 (Bush & Krysan, 2007; Müller *et al.*, 2010) and YODA (Bergmann *et al.*, 2004) in tissues such as the root tip and lateral root primordia. Lateral root primordia and roots are produced by the mature pericycle and this is clearly a post-embryogenic aspect of root development (Benkova & Bielach, 2010). Our studies on lateral roots revealed higher lateral root density and cell division defects in both *yda1* and Δ*Nyda1* mutants.

Exclusively in *yda1* and not in Δ*Nyda1* mutants, we observed that phragmoplasts show delayed expansion. In such cases, daughter nuclei that were already reconstituted and showed perinuclear microtubules were separated by young phragmoplasts. Furthermore, we observed a failure of cell plate completion, resulting in binucleate cells.

Specification of MPK6 downstream of YODA in the regulation of cell division

MPK6 and MPK3 can redundantly regulate stomatal ontogenesis downstream of YODA (Wang *et al.*, 2007). However, MPK6 alone suffices to affect root division patterns similarly to YODA, as *mpk6-2* and *yda1* mutants as well as the *mpk6-4* mutant transformed with *MPK6AEF* show similar cell division plane misorientations (this study and Müller *et al.*, 2010). This suggests that MPK6 alone may be generally involved in central mechanisms regulating cell division. The matter of developmental redundancy of MPK3 and MPK6 was

elegantly addressed by Bush & Krysan (2007), who studied a kinase-dead version of MPK6 (an MPK6 with a TEY motif substituted for AEF) transformed into the *mpk6-4* mutant background. This kinase-dead MPK6 was unable to be phosphorylated and activated, but otherwise capable of undergoing interactions with upstream effectors (Bush & Krysan, 2007). The resulting transgenic line showed stomatal clustering similar to that in *yda.* In this case, although MPK3 is functional, it seems to be displaced by *MPK6AEF* (Bush & Krysan, 2007).

When the phosphorylation status of MPK3 and MPK6 was investigated using the anti-pTEpY antibody, phospho-MPK3 and phospho-MPK6 levels were found to be not only increased in Δ*Nyda1* but quite unexpectedly also in *yda1*. Although this was previously implied (Lampard *et al.*, 2009), it is shown here for the first time. MPK6 recruitment to definite microtubular structures pertinent to cell division plane orientation, such as the PPB and the phragmoplast, seems to be differentially regulated upon YODA perturbation. Thus, in Δ*Nyda1* seedlings, a fraction of MPK6 becomes activated and shows increased association with microtubular structures such as the PPB and the phragmoplast, suggesting that co-localization of MPK6 with PPBs and phragmoplast is probably based on specific YODA-dependent MPK6 activation. By contrast, although *yda1* plants also showed increased levels of phospho-MPK3 and phospho-MPK6, they were notably devoid of MPK6 accumulation in PPBs and phragmoplasts. Perhaps it is related to differential subcellular localization and it will probably require discrimination between nonactive and active pools of MPK3 and MPK6 using monospecific phospho-MAPK antibodies, as was recently described for *Medicago sativa* L. STRESS-INDUCED MITOGEN ACTIVATED PROTEIN KINASE (SIMK) (Ovečka *et al.*, 2014). Unfortunately, commercially available pERK antibodies recognize both activated MPK3 and MPK6.

Cytoskeletal proteins downstream of YODA

Cell division planes are defined by intercellular interactions, hormonal signaling and ultimately coordination of the cortical microtubule to PPB transition (Ten Hove & Heidstra, 2008; van Damme, 2009; Müller *et al.*, 2009; Rasmussen *et al.*, 2011b). To date, definite early markers of PPB definition such as TAN1, POK1 and GCP4 have been described (Panteris, 2008; Müller *et al.*, 2009; Rasmussen *et al.*, 2011b). Here, we showed that *TAN1, POK1* and *GCP4* were differentially expressed in *yda1* and Δ*Nyda1*, which might contribute to deregulated cell division planes in these mutants. Further, nitrilases were overabundant in both mutants and they might provide another link between auxin and cytoskeletal microtubular structures, as NITRILASE1 was shown to localize to the phragmoplast (Doskočilová *et al.*, 2013). In addition, nitrilases were also implicated as playing a role in lateral root development (Kutz *et al.*, 2002).

Microtubule-associated proteins (MAPs) have been confirmed to be tunable regulators of division processes, being phosphorylated by either cyclin-dependent kinases or MAPKs (Binarová *et al.*, 1998; Calderini *et al.*, 1998; Bogre *et al.*, 1999; Smertenko *et al.*, 2006). Arabidopsis MAP65 proteins are ubiquitous MAPs localizing to interphase and mitotic microtubule arrays (Müller *et al.*, 2004; Lucas & Shaw 2012). While single *map65-1* and *map65-2* mutants show no discernible phenotypes, the *map65-1map65-2* double mutant

displays cell proliferation defects (Lucas & Shaw, 2012). In the MAP65 family, MAP65-1, MAP65-2 and MAP65-3 were identified as targets of MPK4 (Beck *et al.*, 2010; Sasabe *et al.*, 2011), whereas MAP65-1 was identified as an MPK6-phosphorylatable protein (Smertenko *et al.*, 2006; Popescu *et al.*, 2009) or substrate (Hoehenwarter *et al.*, 2013). Here we provide co-immunoprecipitation data showing the MPK6 and MAP65-1 interaction (Fig. 13). While total levels of MAP65-1 protein were roughly maintained in Ler, *yda1* and Δ*Nyda1*, the extent of co-localization between MAP65-1 and microtubules was markedly different. Principally, *yda1* mutants showed a stronger association of MAP65-1 with cortical microtubules, PPBs and phragmoplasts, while the respective microtubule arrays in Δ*Nyda1* were poorly decorated with MAP65-1. Considering the proposed role of MAP65-1 phosphorylation in the speed of phragmoplast expansion (Sasabe *et al.*, 2006, Murata *et al.*, 2013), we reason that MAP65-1 overaccumulation in *yda1* phragmoplasts may prohibit the disassembly of lagging microtubule bundles and cause the observed delay in phragmoplast expansion and the failure of complete cell plate formation. In contrast, the depletion of MAP65-1 from phragmoplast microtubules in the Δ*Nyda1* mutant may accelerate phragmoplast expansion. As phragmoplast expansion is corrected by actin/microtubule attachments with cortical sites of final cell plate fusion, its probably faster expansion in Δ*Nyda1* may lead to failure of such adaptive movements and fusion of cell plates to sites outside the PPB region. This extensive co-localization of MAP65-1 with microtubules in *yda1* and the decreased co-localization of MAP65-1 with microtubules in Δ*Nyda1* can be related to differential, YODA-dependent phosphorylation of MAP65-1 by MPK6.

Concluding remarks

There is accumulating evidence that auxin and MAPKs play a decisive role in developmental fate and tissue patterning by spatially defining symmetric and asymmetric divisions (De Smet & Beeckman, 2011; Lau & Bergmann, 2012; Šamajová *et al.*, 2013). Auxin and MAPKs such as MPK4 (Beck *et al.*, 2010, 2011; Sasabe *et al.*, 2011) and MPK6 (Müller *et al.*, 2010) seem to define the spatial orientation of cell division planes, allowing pattern formation of higher plant vegetative organs. Microtubule-associated proteins currently represented by members of the plant MAP65 family are verified MAPK targets (Sasabe *et al.*, 2011). However, more studies are necessary to address the overall cytoskeletal implications of MAPK signaling, as regulatory proteins such as katanin, END BINDING PROTEIN 1 (EB1) and Rho of plants (Rop) are predicted MAPK targets (Šamajová *et al.*, 2013). Here, we showed that genes regulating cell division orientation, such as *TAN1*, *POK1* and *GCP4*, were differentially expressed while nitrilases (including phragmoplast-associated NI-TRILASE1) were up-regulated in the *yda1* and Δ*Nyda1* mutants. Finally, the results presented imply a role of MPK6 downstream of the YODA in the determination of cell division orientation and cytokinesis in Arabidopsis primary and lateral roots. A definite and complete pathway of MAPKs and MAPs, dedicated to the spatial determination of cell division plane merits the attention of future studies.

Supplementary Material

Refer to Web version on PubMed Central for supplementary material.

Acknowledgments

We thank Ulla Mettbach, Jens Muller, Nils Böhm, Martina Beck and Diedrik Menzel for their help in the initial stages of this project. Seeds of *yda* and Δ*Nyda* mutants were kindly provided by Wolfgang Lukowitz. We thank Andrei Smertenko for providing rabbit polyclonal anti-MAP65-1 serum, Ken-ichiro Hayashi for auxinole, Eva Hirnerová for her help with auxin analyses, and Xuan Ding and Tony Arick for their assistance with mass spectrometry data collection and export, respectively. This research was supported by grant no. P501/11/1764 from the Czech Science Foundation GAČR, by the National Program for Sustainability I (grant no. LO1204) provided by the Czech Ministry of Education, and by student grant IGA PrF UP 2014–033, and P.V. was supported by grant CZ. 1.07/2.3.00/30.0041 POSTUP II at Palacký University, Olomouc, Czech Republic. MS-based proteomics analysis was performed at and funded by the Institute for Genomics, Biocomputing and Biotechnology, Mississippi State University.

References

Bartel B, Fink GR. Differential regulation of an auxin-producing nitrilase gene family. Arabidopsis thaliana Proceedings of the National Academy of Sciences, USA. 1994; 91:6649–6653.

Bayer M, Nawy T, Giglione C, Galli M, Meinnel T, Lukowitz W. Paternal control of embryonic patterning in *Arabidopsis thaliana*. Science. 2009; 323:1485–1488. [PubMed: 19286558]

Beck M, Komis G, Müller J, Menzel D, Šamaj J. Arabidopsis homologs of nucleus-and phragmoplast-localized kinase 2 and 3 and mitogen-activated protein kinase 4 are essential for microtubule organization. Plant Cell. 2010; 22:755–771. [PubMed: 20215588]

Beck M, Komis G, Ziemann A, Menzel D, Šamaj J. Mitogen-activated protein kinase 4 is involved in the regulation of mitotic and cytokinetic microtubule transitions in *Arabidopsis thaliana*. New Phytologist. 2011; 189:1069–1083. [PubMed: 21155826]

Benková E, Bielach A. Lateral root organogenesis – from cell to organ. Current Opinion Plant Biology. 2010; 13:677–683.

Bergmann DC, Lukowitz W, Somerville CR. Stomatal development and pattern controlled by a MAPKK kinase. Science. 2004; 304:1494–1497. [PubMed: 15178800]

Binarová P, Dolezel J, Draber P, Heberle-Bors E, Strnad M, Bögre L. Treatment of *Vicia faba* root tip cells with specific inhibitors to cyclin-dependent kinases leads to abnormal spindle formation. Plant Journal. 1998; 16:697–707. [PubMed: 10069076]

Bögre L, Calderini O, Binarova P, Mattauch M, Till S, Kiegerl S, Jonak C, Pollaschek C, Barker P, Huskisson NS, et al. A MAP kinase is activated late in plant mitosis and becomes localized to the plane of cell division. Plant Cell. 1999; 11:101–113. [PubMed: 9878635]

Breuninger H, Lenhard M. Control of tissue and organ growth in plants. Current Topics in Developmental Biology. 2010; 91:185–220. [PubMed: 20705183]

Buschmann H, Chan J, Sanchez-Pulido L, Andrade-Navarro MA, Doonan JH, Lloyd CW. Microtubule-associated AIR9 recognizes the cortical division site at preprophase and cell-plate insertion. Current Biology. 2006; 16:1938–1943. [PubMed: 17027491]

Buschmann H, Hauptmann M, Niessing D, Lloyd CW, Schäffner AR. Helical growth of the Arabidopsis mutant *tortifolia2* does not depend on cell division patterns but involves handed twisting of isolated cells. Plant Cell. 2009; 21:2090–2106. [PubMed: 19638477]

Bush SM, Krysan PJ. Mutational evidence that the Arabidopsis MAP kinase MPK6 is involved in anther, inflorescence, and embryo development. Journal of Experimental Botany. 2007; 58:2181–2191. [PubMed: 17519351]

Calderini O, Bögre L, Vicente O, Binarova P, Heberle-Bors E, Wilson C. A cell cycle regulated MAP kinase with a possible role in cytokinesis in tobacco cells. Journal of Cell Science. 1998; 111:3091–3100. [PubMed: 9739082]

Colcombet J, Hirt H. Arabidopsis MAPKs: a complex signalling network involved in multiple biological processes. BiochemicalJournal. 2008; 413:217–226. [PubMed: 18570633]

van Damme D. Division plane determination during plant somatic cytokinesis. Current Opinion in Plant Biology. 2009; 12:745–751. [PubMed: 19850508]

De Smet I. Lateral root initiation: one step at a time. New Phytologist. 2012; 193:867–873. [PubMed: 22403823]

De Smet I, Beeckman T. Asymmetric cell division in land plants and algae: the driving force for differentiation. Nature Reviews Molecular Cell Biology. 2011; 12:177–188.

Dhonukshe P, Mathur J, Hülskamp M, Gadella TW Jr. Microtubule plus-ends reveal essential links between intracellular polarization and localized modulation of endocytosis during division-plane establishment in plant cells. BMC Biology. 2005; 3:11. [PubMed: 15831100]

Doskočilová A, Kohoutová L, Volc J, Kourová H, Benada O, Chumová J, Plihal O, Petrovská B, Halada P, Bögre L, et al. NITRILASE1 regulates the exit from proliferation, genome stability and plant development. New Phytologist. 2013; 198:685–698. [PubMed: 23437871]

Dubrovsky J, Sauer M, Napsucialy-Mendivil S, Ivanchenko MG, Friml J, Shishkova S, Celenza J, Benkova E. Auxin acts as a local morphogenetic trigger to specify lateral root founder cells. Proceedings of the National Academy of Sciences, USA. 2008; 105:8790–8794.

Fujita S, Pytela J, Hotta T, Kato T, Hamada T, Akamatsu R, Ishida Y, Kutsuna N, Hasezawa S, Nomura Y, et al. An atypical tubulin kinase mediates stress-induced microtubule depolymerization in Arabidopsis. Current Biology. 2013; 23:1969–1978. [PubMed: 24120637]

Furutani I, Watanabe Y, Prieto R, Masukawa M, Suzuki K, Naoi K, Thitamadee S, Shikanai T, Hashimoto T. The *SPIRAL* genes are required for directional control of cell elongation in *Arabidopsis thaliana*. Development. 2000; 127:4443–4453. [PubMed: 11003843]

Goh T, Voβ U, Farcot E, Bennett MJ, Bishopp A. Systems biology approaches to understand the role of auxin in root growth and development. Physiologia Plantarum. 2014; 151:73–78. [PubMed: 24494934]

Hayashi K, Nave J, Zheng N, Hirose M, Kuboki A, Shimada Y, Kepinski S, Nozaki H. Rational design of an auxin antagonist of the SCF^{TIR1} auxin receptor complex. ACS Chemical Biology. 2012; 7:590–598. [PubMed: 22234040]

Hayashi K, Tan X, Zheng N, Hatate T, Kimura Y, Kepinski S, Nozaki H. Small-molecule agonists and antagonists of F-box protein-substrate interactions in auxin perception and signaling. Proceedings of the National Academy of Sciences, USA. 2008; 105:5632–5637.

Higaki T, Kutsuna N, Sano T, Hasezawa S. Quantitative analysis of changes in actin microfilament contribution to cell plate development in plant cytokinesis. BMC Plant Biology. 2008; 8:80. [PubMed: 18637163]

Hoehenwarter W, Thomas M, Nukarinen E, Egelhofer V, Röhrig H, Weckwerth W, Conrath U, Beckers GJ. Identification of novel *in vivo* MAP kinase substrates in *Arabidopsis thaliana* through use of tandem metal oxide affinity chromatography. Molecular & Cell Proteomics. 2013; 12:369–380.

Hofhuis H, Laskowski M, Du Y, Prasad K, Grigg S, Pinon V, Scheres B. Phyllotaxis and rhizotaxis in Arabidopsis are modified by three PLETHORA transcription factors. Current Biology. 2013; 23:956–962. [PubMed: 23684976]

Ishida T, Kaneko Y, Iwano M, Hashimoto T. Helical microtubule arrays in a collection of twisting tubulin mutants of *Arabidopsis thaliana*. Proceeding of the National Academy of Sciences, USA. 2007; 104:8544–8549.

Jensen LJ, Kuhn M, Stark M, Chaffron S, Creevey C, Muller J, Doerks T, Julien P, Roth A, Simonovic M, et al. STRING 8-a global view on proteins and their functional interactions in 630 organisms. Nucleic Acids Research. 2009; 37:D412–D416. [PubMed: 18940858]

Karahara I, Suda J, Tahara H, Yokota E, Shimmen T, Misaki K, Yonemura S, Staehelin LA, Mineyuki Y. The preprophase band is a localized center of clathrin-mediated endocytosis in late prophase cells of the onion cotyledon epidermis. Plant Journal. 2009; 57:819–831. [PubMed: 18980648]

Kim TW, Michniewicz M, Bergmann DC, Wang ZY. Brassinosteroid regulates stomatal development by GSK3-mediated inhibition of a MAPK pathway. Nature. 2012; 482:419–422. [PubMed: 22307275]

Kirik A, Ehrhardt DW, Kirik V. TONNEAU2/FASS regulates the geometry of microtubule nucleation and cortical array organization in interphase Arabidopsis cells. Plant Cell. 2012; 24:1158–1170. [PubMed: 22395485]

Komis G, Illés P, Beck M, Šamaj J. Microtubules and mitogen-activated protein kinase signalling. Current Opinion in Plant Biology. 2011; 14:650–657. [PubMed: 21839668]

Kong Z, Hotta T, Lee YR, Horio T, Liu B. The γ-tubulin complex protein GCP4 is required for organizing functional microtubule arrays in *Arabidopsis thaliana*. Plant Cell. 2010; 22:191–204. [PubMed: 20118227]

Kosetsu K, Matsunaga S, Nakagami H, Colcombet J, Sasabe M, Soyano T, Takahashi Y, Hirt H, Machida Y. The MAP kinase MPK4 is required for cytokinesis in *Arabidopsis thaliana*. Plant Cell. 2010; 22:3778–3790. [PubMed: 21098735]

Kutz A, Müller A, Hennig P, Kaiser WM, Piotrowski M, Weiler EW. A role for nitrilase 3 in the regulation of root morphology in sulphur-starving *Arabidopsis thaliana*. Plant Journal. 2002; 30:95–106. [PubMed: 11967096]

Lampard GR, Lukowitz W, Ellis BE, Bergmann DC. Novel and expanded roles for MAPK signaling in Arabidopsis stomatal cell fate revealed by cell type-specific manipulations. Plant Cell. 2009; 21:3506–3517. [PubMed: 19897669]

Lau OS, Bergmann DC. Stomatal development: a plant's perspective on cell polarity, cell fate transitions and intercellular communication. Development. 2012; 139:3683–3692. [PubMed: 22991435]

Lloyd C, Chan J. The parallel lives of microtubules and cellulose microfibrils. Current Opinion in Plant Biology. 2008; 11:641–646. [PubMed: 18977684]

Lucas JR, Shaw SL. MAP65-1 and MAP65-2 promote cell proliferation and axial growth in Arabidopsis roots. Plant Journal. 2012; 71:454–463. [PubMed: 22443289]

Lukowitz W, Roeder A, Parmenter D, Somerville C. A MAPKK kinase gene regulates extra-embryonic cell fate in Arabidopsis. Cell. 2004; 116:109–119. [PubMed: 14718171]

Mao G, Chan J, Calder G, Doonan JH, Lloyd CW. Modulated targeting of GFP-AtMAP65-1 to central spindle microtubules during division. Plant Journal. 2005; 43:469–478. [PubMed: 16098102]

Mashiguchi K, Tanaka K, Sakai T, Sugawara S, Kawaide H, Natsume M, Hanada A, Yaeno T, Shirasu K, Yao H, et al. The main auxin biosynthesis pathway in Arabidopsis. Proceedings of the National Academy of Sciences, USA. 2011; 108:18512–18517.

Muller J, Beck M, Mettbach U, Komis G, Hause G, Menzel D, Šamaj J. Arabidopsis MPK6 is involved in cell division plane control during early root development, and localizes to the pre-prophase band, phragmoplast, trans-Golgi network and plasma membrane. Plant Journal. 2010; 61:234–248. [PubMed: 19832943]

Müller S, Han S, Smith LG. Two kinesins are involved in the spatial control of cytokinesis in *Arabidopsis thaliana*. Current Biology. 2006; 16:888–894. [PubMed: 16682350]

Müller S, Smertenko A, Wagner V, Heinrich M, Hussey PJ, Hauser MT. The plant microtubule-associated protein AtMAP65–3/PLE is essential for cytokinetic phragmoplast function. Current Biology. 2004; 14:412–417. [PubMed: 15028217]

Müller S, Wright AJ, Smith LG. Division plane control in plants: new players in the band. Trends in Cell Biology. 2009; 19:180–188. [PubMed: 19285867]

Murata T, Sano T, Sasabe M, Nonaka S, Higashiyama T, Hasezawa S, Machida Y, Hasebe M. Mechanism of microtubule array expansion in the cytokinetic phragmoplast. Nature Communications. 2013; 4:1967.

Nadeau JA. Stomatal development: new signals and fate determinants. Current Opinion in Plant Biology. 2009; 12:29–35. [PubMed: 19042149]

Novák O, Hényková E, Sairanen I, Kowalczyk M, Pospíšil T, Ljung K. Tissue-specific profiling of the *Arabidopsis thaliana* auxin metabolome. Plant Journal. 2012; 72:523–536. [PubMed: 22725617]

Okushima Y, Overvoorde PJ, Arima K, Alonso JM, Chan A, Chang C, Ecker JR, Hughes B, Lui A, Nguyen D, et al. Functional genomic analysis of the *AUXIN RESPONSE FACTOR gene* family members in *Arabidopsis thaliana*: unique and overlapping functions of *ARF7* and *ARF19*. Plant Cell. 2005; 17:444–463. [PubMed: 15659631]

Ovečka M, Takáč T, Komis G, Vadovič P, Bekešová S, Doskočilová A, Smékalova V, Luptovčiak I, Šamajová O, Schweighofer A, et al. Salt-induced subcellular kinase relocation and seeding susceptibility caused by overexpression of Medicago SIMKK in Arabidopsis. Journal of Experimental Botany. 2014; 65:2335–2350. [PubMed: 24648569]

Panteris E. Cortical actin filaments at the division site of mitotic plant cells: a reconsideration of the 'actin-depleted zone'. New Phytologist. 2008; 179:334–341. [PubMed: 19086286]

Popescu SC, Popescu GV, Bachan S, Zhang Z, Gerstein M, Snyder M, Dinesh-Kumar SP. MAPK target networks in *Arabidopsis thaliana* revealed using functional protein microarrays. Genes & Development. 2009; 23:80–92. [PubMed: 19095804]

Qian P, Hou S, Guo G. Molecular mechanisms controlling pavement cell shape in Arabidopsis leaves. Plant Cell Reports. 2009; 28:1147–1157. [PubMed: 19529941]

Rasmussen CG, Humphries JA, Smith LG. Determination of symmetric and asymmetric division planes in plant cells. Annual Review of Plant Biology. 2011a; 62:387–409.

Rasmussen CG, Sun B, Smith LG. Tangled localization at the cortical division site of plant cells occurs by several mechanisms. Journal of Cell Science. 2011b; 124:270–279. [PubMed: 21172800]

Rasmussen MW, Roux M, Petersen M, Mundy J. MAP kinase cascades in Arabidopsis innate immunity. Frontiers in Plant Sciences. 2012; 3:169.

Šamajová O, Komis G, Šamaj J. Emerging topics in the cell biology of mitogen-activated protein kinases. Trends in Plant Science. 2013; 18:40–48.

Sasabe M, Kosetsu K, Hidaka M, Murase A, Machida Y. *Arabidopsis thaliana* MAP65-1 and MAP65-2 function redundantly with MAP65-3/PLEIADE in cytokinesis downstream of MPK4. Plant Signaling and Behavior. 2011; 6:743–747. [PubMed: 21455028]

Sasabe M, Machida Y. Regulation of organization and function of microtubules by the mitogen-activated protein kinase cascade during plant cytokinesis. Cytoskeleton (Hoboken). 2012; 69:913–918. [PubMed: 23027702]

Sasabe M, Soyano T, Takahashi Y, Sonobe S, Igarashi H, Itoh TJ, Hidaka M, Machida Y. Phosphorylation of NtMAP65-1 by a MAP kinase down-regulates its activity of microtubule bundling and stimulates progression of cytokinesis of tobacco cells. Genes & Development. 2006; 20:1004–1014. [PubMed: 16598040]

Sedbrook JC, Ehrhardt DW, Fisher SE, Scheible WR, Somerville CR. The Arabidopsis *SKU6/SPIRAL1* gene encodes a plus end-localized microtubule-interacting protein involved in directional cell expansion. Plant Cell. 2004; 16:1506–1520. [PubMed: 15155883]

Smertenko AP, Chang HY, Sonobe S, Fenyk SI, Weingartner M, Bögre L, Hussey PJ. Control of the AtMAP65-1 interaction with microtubules through the cell cycle. Journal of Cell Science. 2006; 119:3227–3237. [PubMed: 16847052]

Szymanski DB, Cosgrove DJ. Dynamic coordination of cytoskeletal and cell wall systems during plant cell morphogenesis. Current Opinion in Plant Biology. 2009; 19:R800–R811.

Ten Hove CA, Heidstra R. Who begets whom? Plant cell fate determination by asymmetric cell division. Current Opinion in Plant Biology. 2008; 11:34–41. [PubMed: 18162432]

Tian C, Muto H, Higuchi K, Matamura T, Tatematsu K, Koshiba T, Yamamoto KT. Disruption and overexpression of *auxin response factor 8* gene of Arabidopsis affect hypocotyl elongation and root growth habit, indicating its possible involvement in auxin homeostasis in light condition. Plant Journal. 2004; 40:333–343. [PubMed: 15469491]

Tominaga-Wada R, Ishida T, Wada T. New insights into the mechanism of development of Arabidopsis root hairs and trichomes. International Review of Cell and Molecular Biology. 2011; 286:67–106. [PubMed: 21199780]

Walia A, Lee JS, Wasteneys G, Ellis B. Arabidopsis mitogen-activated protein kinase MPK18 mediates cortical microtubule functions in plant cells. Plant Journal. 2009; 59:565–575. [PubMed: 19392697]

Walker KL, Müller S, Moss D, Ehrhardt DW, Smith LG. Arabidopsis TANGLED identifies the division plane throughout mitosis and cytokinesis. Current Biology. 2007; 17:1827–1836. [PubMed: 17964159]

Wang H, Ngwenyama N, Liu Y, Walker JC, Zhang S. Stomatal development and patterning are regulated by environmentally responsive mitogen-activated protein kinases in Arabidopsis. Plant Cell. 2007; 19:63–73. [PubMed: 17259259]

Xu XM, Zhao Q, Rodrigo-Peiris T, Brkljacic J, He CS, Müller S, Meier I. RanGAP1 is a continuous marker of the Arabidopsis cell division plane. Proceedings of the National Academy of Sciences, USA. 2008; 105:18637–18642.

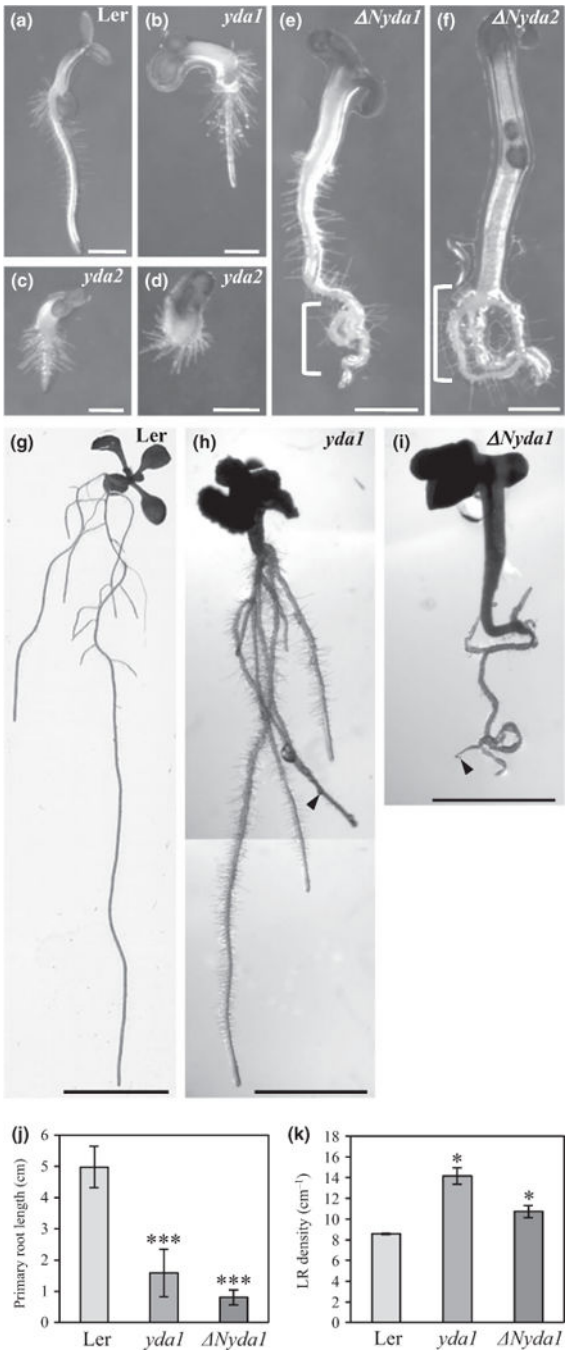

Fig. 1.

Phenotypes of primary roots, lateral roots and root hairs in the *yda1* and Δ*Nyda1* mutants. (a–f) Primary root development of 4-d-old Arabidopsis seedlings of Landsberg erecta (Ler) (a), *yda1* (b), *yda2* (c, d), Δ*Nyda1* (e) and Δ*Nyda2* (f). *yda* mutants show disturbed primary root growth resulting in thickened, short roots compared with Ler (b–d; cf. a). By contrast, Δ*Nyda1* mutants show promoted root elongation and in some cases curling of primary roots (e, f, brackets). (g–i) Overview of lateral and adventitious roots of 8-d-old seedlings of Ler (g), *yda1* (h) and Δ*Nyda1* (i). Both *yda1* and Δ*Nyda1* mutants showed shorter primary roots

in comparison to Ler (g; cf. h, i). (j, k) Quantitative evaluation of primary root lengths (j) and lateral root (LR) density (k) of 8-d-old Ler, *yda1* and Δ*Nyda1* seedlings. Lateral root density was obtained from the root branching zone of the wild-type and both mutants. Bar charts represent the mean ± SD for Ler ($N = 21$), *yda1* ($N = 12$) and Δ*Nyda1* ($N = 19$). *, $P<0.05$; ***, $P< 0.001$. Arrowheads (h, i) mark the apex of the primary root. Bars: (a–d) 0.5 mm; (e, f) 1 mm; (g) 1 cm; (h, i) 2 mm.

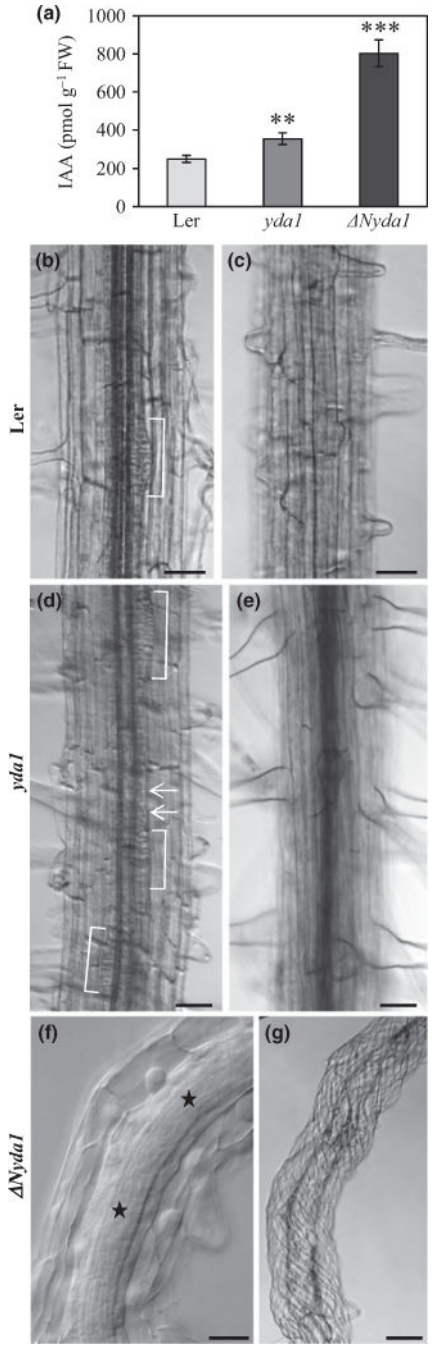

Fig. 2.

Endogenous indole-3-acetic acid (IAA) content and primary root phenotype of Landsberg erecta (Ler), *yda1* and Δ*Nyda1* plants. (a) Quantitative determination (mean ± SD, $N = 4$ for all cases examined) of endogenous IAA concentration in whole plants of Ler, *yda1* and Δ*Nyda1*. Fourteen-day-old Arabidopsis plants cultivated in standard light conditions, but with dark-grown roots, were analyzed in two independent experiments with four biological replicates. **, $P<0.01$; ***, $P< 0.001$. (b–g) Root morphology of 14-d-old Ler, *yda1* and Δ*Nyda1* plants. Median (b, d, f) and surface (c, e, g) views of a mature part of the primary

root are shown. In Ler, lateral root primordial emerged at regular intervals (b). In *yda1*, lateral root primordia developed at a higher density (d, brackets), and some additional ectopic cell divisions in the pericycle were observed (d, arrows). In both Ler and *yda1*, cell files were arranged parallel to the longitudinal axis of the root (c, e). In Δ*Nyda1*, ectopic cell divisions were frequent in both the central cylinder and the pericycle (f, asterisks) and cell files were extensively twisted (g). Bars: (b–e, g) 50 μm; (f) 20 μm.

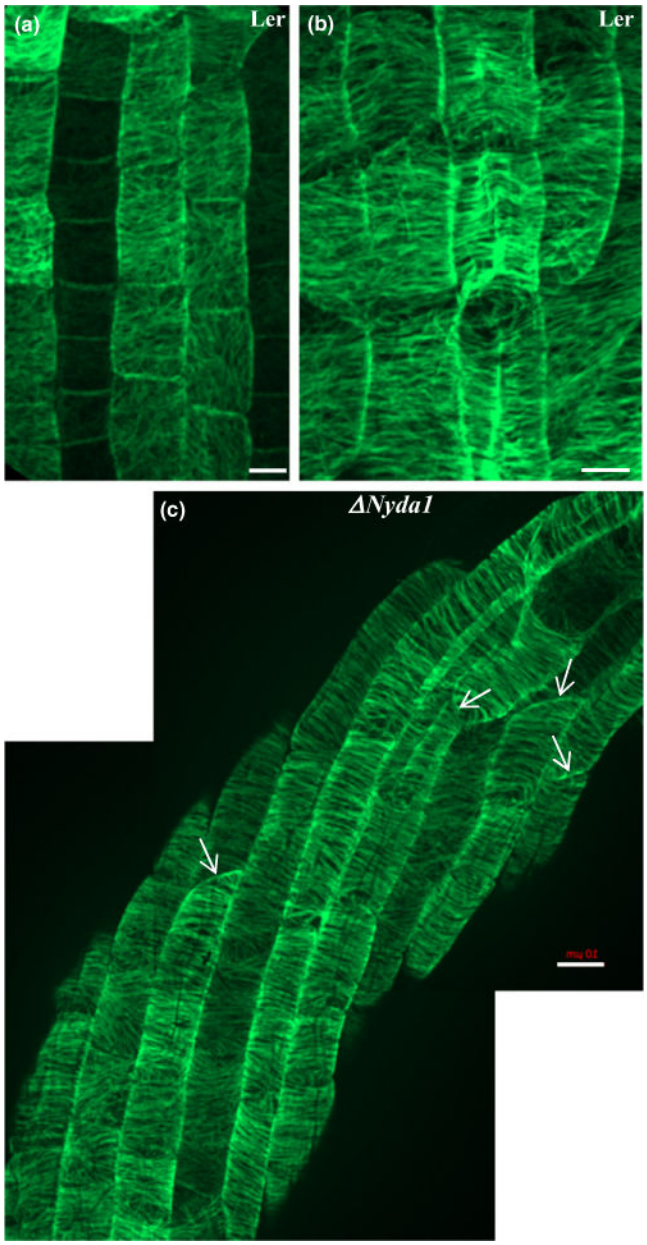

Fig. 3.

Organization of cortical microtubules in interphase epidermal cells of the primary roots of Landsberg erecta (Ler) and Δ*Nyda1* Arabidopsis plants after tubulin immunolocalization in root wholemounts and CLSM. (a, b) Transition and elongation zones in roots of Ler. In the transition zone of the root (a), cells in the rootward direction had cortical microtubules randomly oriented, while in cells in the shootward direction, cortical microtubules were gradually rearranged into a loosely transversal orientation. In the elongation zone (b), cortical microtubules in all cells had a transversal orientation. (c) Cortical microtubules in root cells of the Δ*Nyda1* mutant. In contrast to the extensive twisting of elongating root epidermal cells, cortical microtubules kept a normal transversal orientation. Oblique cross

cell walls between neighboring cells in epidermal cell files are indicated by arrows (c). The root tip direction is at the bottom of the figures. Bars, 10 μm.

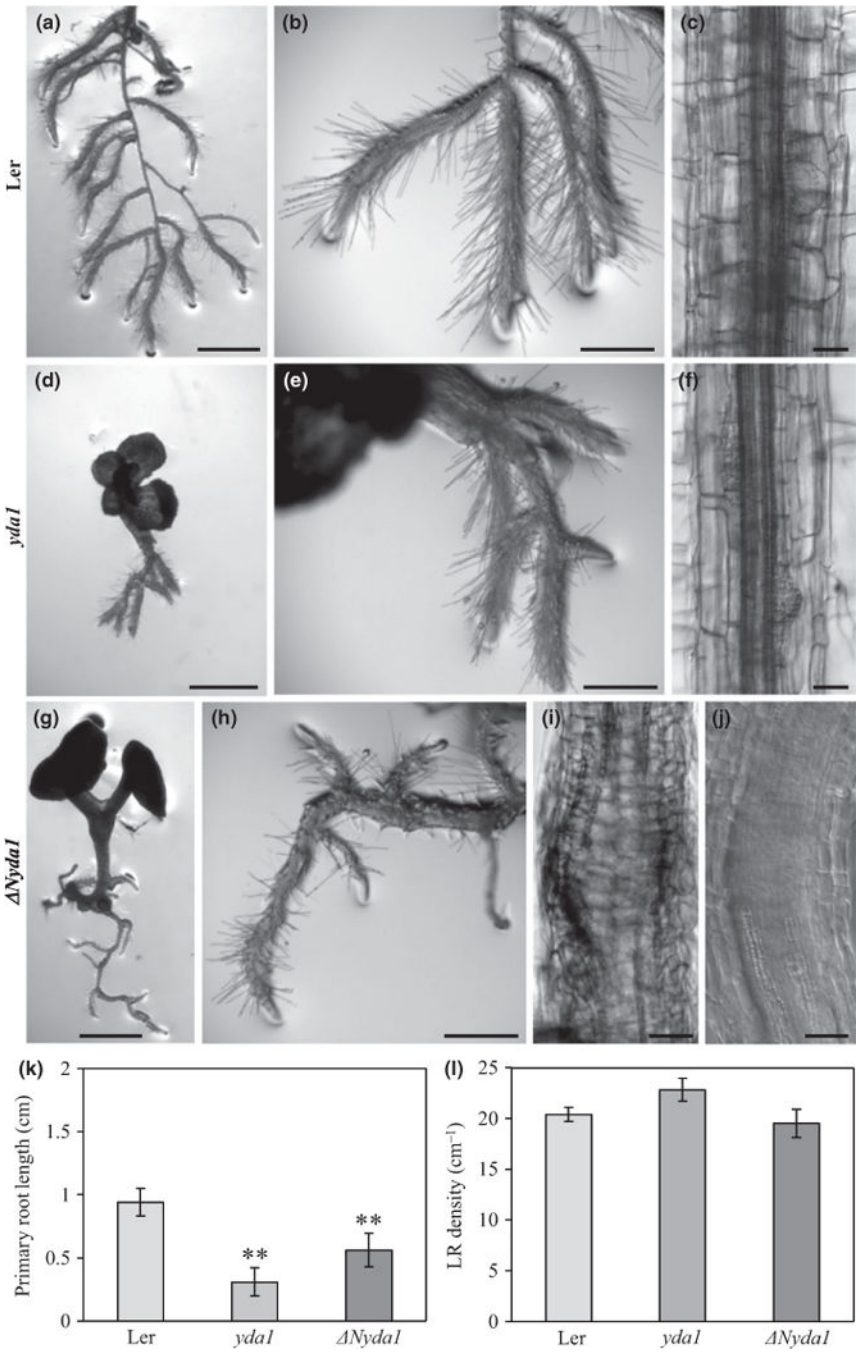

Fig. 4.

Effects of external indole-3-acetic acid (IAA) on the root phenotype of Landsberg erecta (Ler), *yda1* and Δ*Nyda1* Arabidopsis plants. (a–j) Root morphology of plants grown on medium containing 1 μM IAA. In Ler, the root system consisted of excessively branched primary roots with lateral roots of equal length (a, b). IAA reduced the elongation of root cells and induced the formation of lateral root primordia (c). Roots of *yda1* were short (d) and formed lateral roots (e) and lateral root primordia (f) close to each other. Δ*Nyda1* plants developed a root system with regularly spaced lateral roots (g, h). External IAA did not

induce enhanced formation of lateral root primordia in Δ*Nyda1* plants. Instead, massive ectopic cell division was locally induced in the central cylinder, which even interfered with regular differentiation of vascular cell files (i, j). Plants 3-d-old were transferred to medium containing 1 μM IAA and examined 5 d after transfer (a, b, d, e, g, h) and 11 d after transfer (c, f, i, j). (k, l) Quantitative evaluation of primary root lengths (k) and lateral root density (l) of 8-d-old Ler, *yda1* and Δ*Nyda1* seedlings. Lateral root density was obtained from the root branching zone of the wild-type and both mutants. Bar charts represent the mean ± SD for Ler (N = 21), *yda1* (N = 14) and Δ*Nyda1* (N= 14).**, $P < 0.01$. Bars: (a, d, g) 1 mm; (b, e, h) 500 μm; (c, f, i) 50 μm; (j) 20 μm.

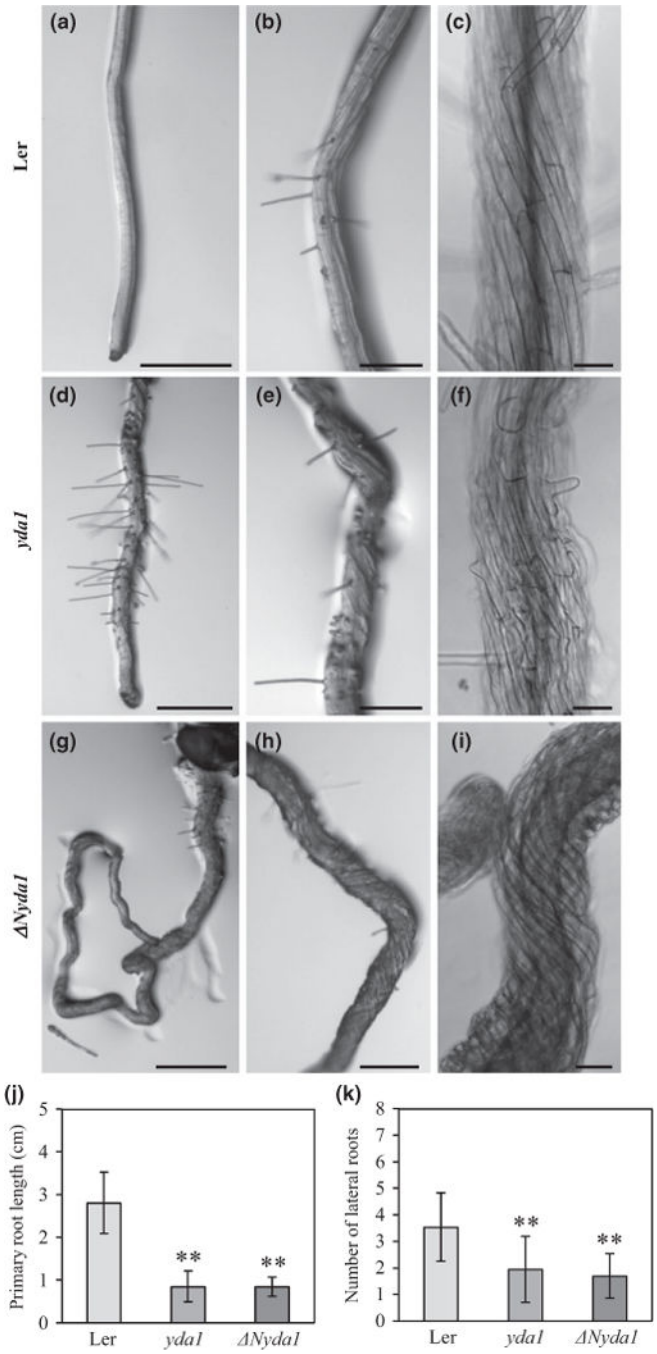

Fig. 5.

Effects of auxinole (α-(2,4-dimethylphenylethyl-2-oxo)-IAA) on the root phenotype of Landsberg erecta (Ler), *yda1* and Δ*Nyda1* Arabidopsis plants. (a–i) Primary root morphology of plants grown on medium containing 10μM auxinole. Roots of all three lines exhibited agravitropic growth, reduced formation of root hairs and reduced branching. In Ler, moderate twisting of the root was induced (a–c). Root twisting in *yda1* plants was more pronounced (d–f) and excessive twisting of Δ*Nyda1* plants was not affected by auxinole (g–i). Plants 3-d-old were transferred to medium containing 10μM auxinole and examined 5 d

after transfer (a, b, d, e, g, h) and 11 d after transfer (c, f, i). (j, k) Quantitative evaluation of primary root lengths (j) and number of lateral roots (k) of 8-d-old Ler, *yda1* and Δ*Nyda1* seedlings. Bar charts represent the mean ± SD for Ler (*N*= 18), *yda1* (*N* = 14) and Δ*Nyda1* (*N* = 20). **, *P*<0.01. Bars: (a, d, g) 500 μm; (b, e, h) 200 μm; (c, f, i) 50 μm.

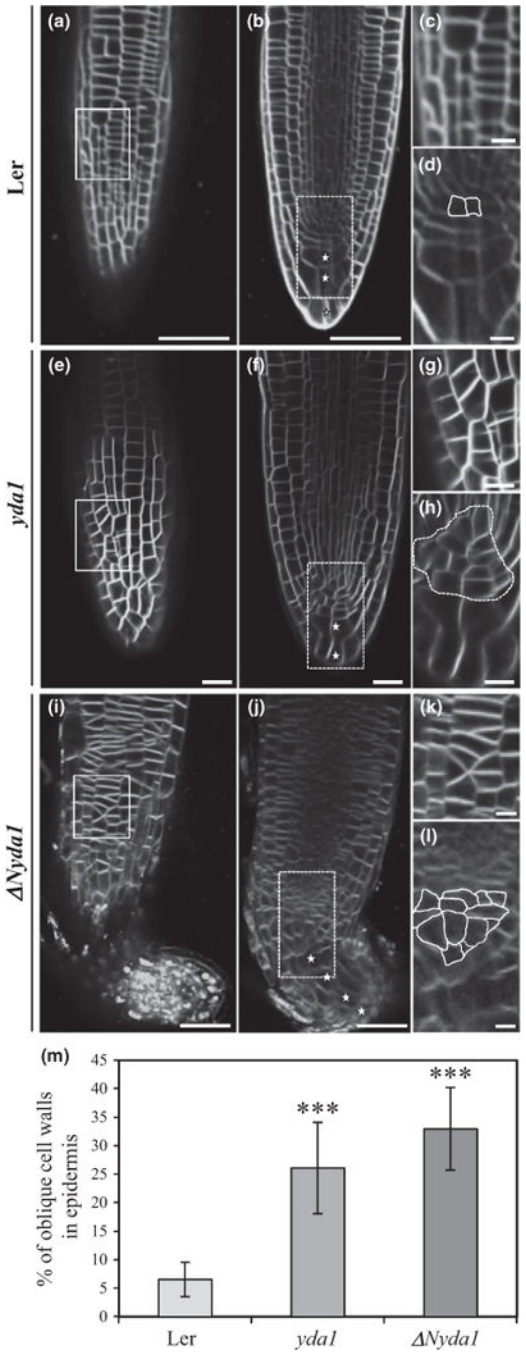

Fig. 6.

Primary root cell architecture in Landsberg erecta (Ler), *yda1* and Δ*Nyda1* Arabidopsis plants after staining of living roots with membrane marker FM4-64 and CLSM. (a–d) Surface (a, c) and central (b, d) optical sections of a Ler root. (a) Overview and (c) higher magnification of the epidermis showing the orderly arrangement of epidermal cells in linear files resulting from symmetric periclinal and anticlinal divisions in Ler. (b) Overview and (d) higher magnification of an orderly structured stem cell niche region in Ler. (e–h) Surface (e, g) and central (f, h) optical sections of a *yda1* root at similar planes as shown in (a)–(d).

(e) Overview and (g) higher magnification of the epidermis showing disturbed cell division planes. Similarly, in central sections (f, h) the stem cell niche is disordered with ectopic cell divisions and displaced cell division planes. (i–l) Surface (i, k) and central (j, l) sections of a Δ*Nyda1* root. (i, k) Epidermal cell divisions are severely disordered with aberrant, oblique cell division planes. The stem cell niche (j, l) shows similarly defective organization with ectopic cell divisions and altered cell division planes as in *yda1*. (m) Quantification of oblique cell walls graphically depicting mean ± SD for Ler ($N = 610$), *yda1* ($N = 645$) and Δ*Nyda1* ($N = 596$). Cell walls were evaluated in 10 independent plants in each case. White asterisks in (b, f, j) mark root cap layers. ***, $P < 0.001$. Bars: (a, b, i, j) 50 μm; (e, f) 20 μm; (c, d, g, h, k, l) 10 μm.

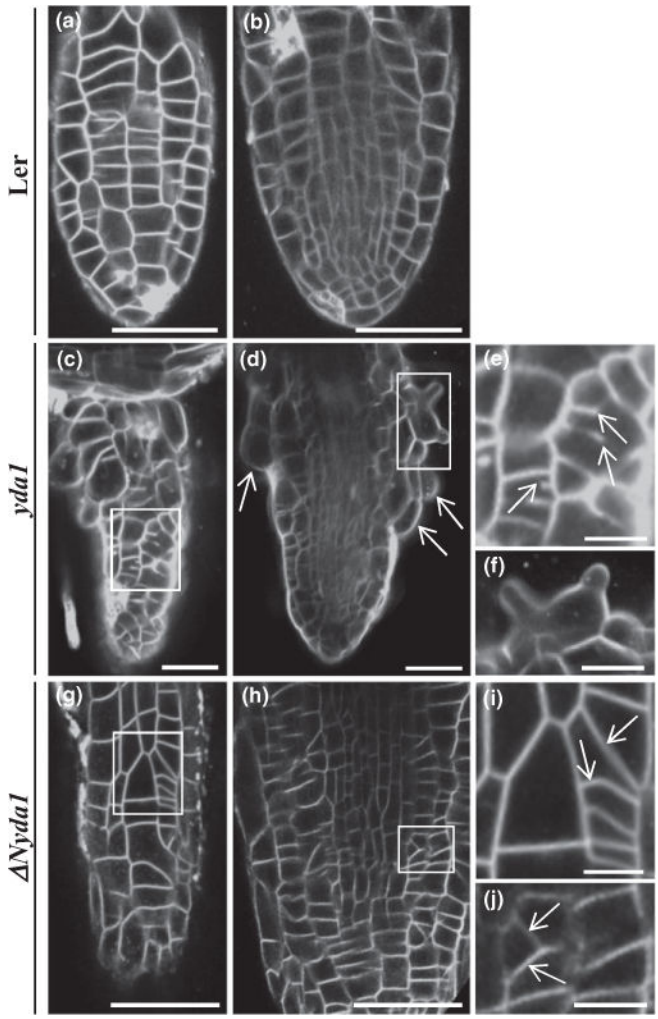

Fig. 7.

Cell division patterns as visualized in young emerging lateral roots of Arabidopsis Landsberg erecta (Ler), *yda1* and Δ*Nyda1* stained with membrane marker FM4-64 and imaged with CLSM. (a, b) Epidermal (a) and central (b) optical sections of a lateral root of Ler showing the fairly ordered cell arrangement of epidermal and central lateral root tissues. (c, d) Epidermal (c) and central (d) optical sections of a *yda1* lateral root exhibiting abnormal cell patterning (c) and bulging of epidermal cells (d, arrows). (e) Higher magnification of the outlined area in (c) showing incomplete cell plate formation in two cells (arrows). (f) Higher magnification of the outlined area in (d) showing a radially expanded trichoblast with two emerging bulges. (g, h) Epidermal (g) and central (h) optical sections of the same Δ*Nyda1* lateral root showing variably disturbed cell division planes (outlined areas). (i, j) Magnified views of the respective outlined areas in (g) and (h) showing oblique cell plates (arrows). Bars: (a–d, g, h) 50 μm; (e, f, i, j) 10 μm.

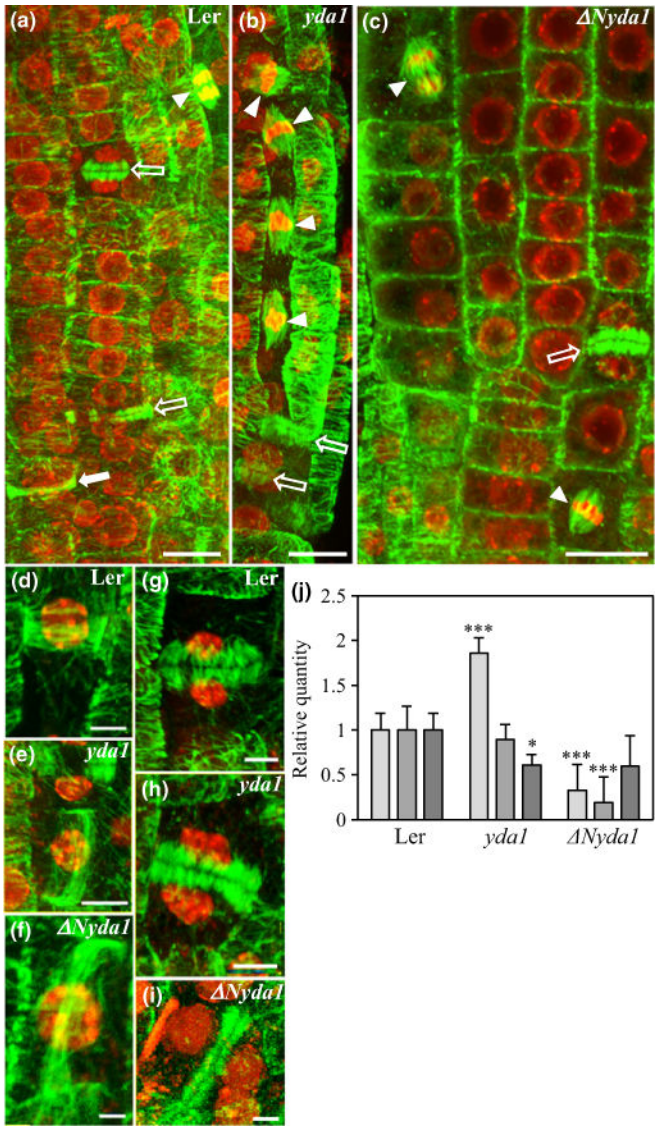

Fig. 8.

Overview of mitotic and cytokinetic microtubule arrays of Arabidopsis Landsberg erecta (Ler), *yda1* and Δ*Nyda1* root whole mounts immunostained for tubulin (green) and counterstained with the DNA stain DAPI (red pseudocolor). (a) Epidermal meristematic region of Ler root showing two cytokinetic cells with phragmoplasts (outlined white arrows), one preprophase cell with preprophase band (PPB; full white arrow) and an anaphase cell with a spindle (arrowhead). (b) An array of synchronously dividing *yda1* root epidermal cells with metaphase spindles (arrowheads) the top one of which is tilted. Outlined white arrows show two cytokinetic cells with phragmoplasts. (c) Part of the meristematic root epidermal area in Δ*Nyda1*. Arrowheads denote two metaphase spindles, one of which is transversely oriented. The outlined arrow shows a phragmoplast. (d–f) Typical, transversely oriented PPB of a Ler preprophase epidermal root cell as compared with oblique PPB formation in *yda1* (e) and Δ*Nyda1* (f). (g–i) Perpendicular phragmoplast in a Ler cytokinetic epidermal cell (g) and oblique phragmoplasts in *yda1* (h) and Δ*Nyda1*

(i). (j) Expression levels of TAN1 (light gray bars), POK1 (mid gray bars) and GCP4 (dark gray bars) genes in extracts from Ler, *yda1* and Δ*Nyda1* plants. The graph shows TAN1, POK1 and GCP4 transcript levels (mean ± SD) quantified by qPCR and normalized against EF1a transcripts. *, $P<0.05$; ***, $P<0.001$. Bars: (a–c) 10 μm; (e) 5 μm; (d, g, h) 3.3 μm; (f) 1.5 μm; (i) 2.5 μm.

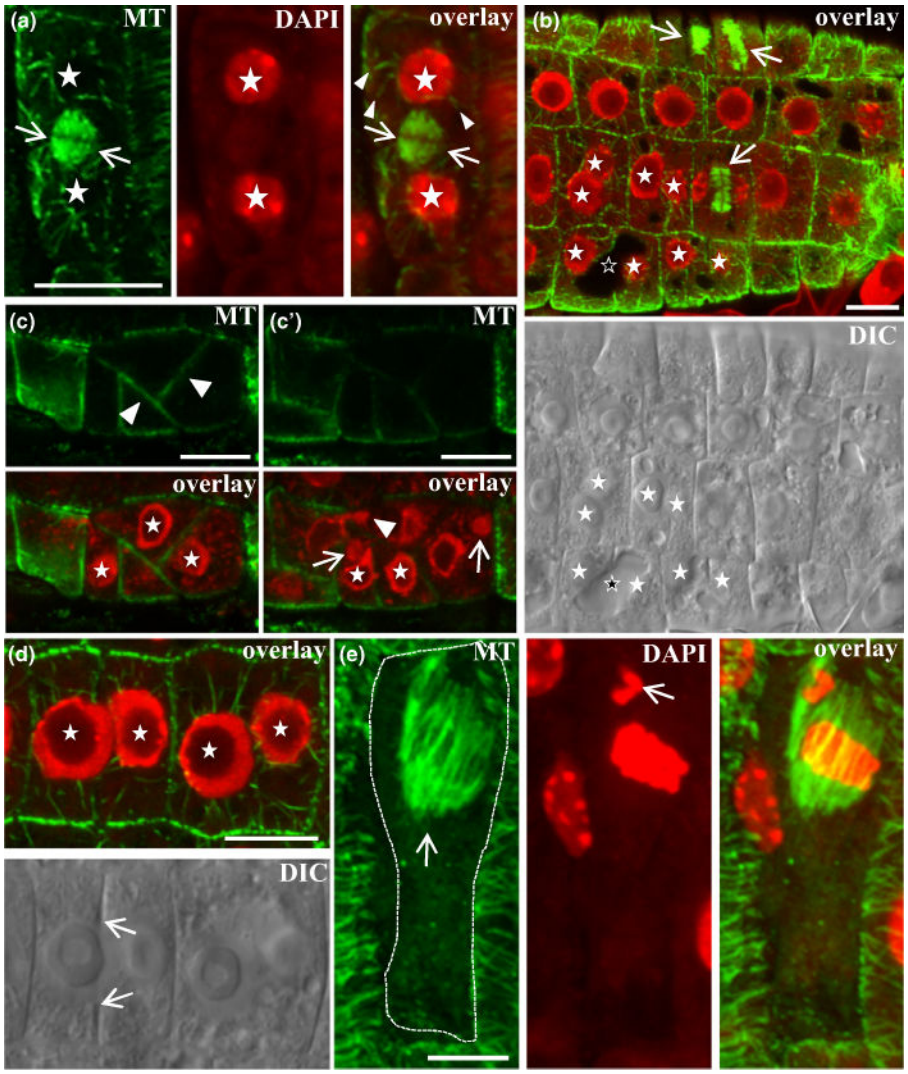

Fig. 9.

Cell division defects in Arabidopsis *yda1* root epidermal cells immunostained for tubulin, counterstained for DNA with DAPI (red pseudocolor), or visualized with differential interference contrast (DIC) optics. (a) Magnification of an epidermal cell showing reconstituted daughter nuclei (asterisks) with perinuclear microtubules (arrowheads) separated by a young phragmoplast (arrows). (b) Immunofluorescent and DIC identification of binucleate cells (nuclei marked with full white asterisks) with incomplete cell plate formation. Arrows point to phragmoplasts. The outlined asterisk marks a vacuole in a binucleate cell which failed to form a cell plate. (c, c′) Different focal planes of an abnormal epidermal cell cluster showing oblique crosswall formation (arrowheads in c) and incomplete cytokinesis. (c′) One nucleus forms a protrusion from one cell compartment to the next (arrowhead) while two cells contain micronuclei (arrows). (d) Immunofluorescent and DIC images of two adjacent binucleate root epidermal cells. Asterisks mark nuclei while arrows point to the margins of an incomplete cell plate. (e) Elongated epidermal cell with ectopically positioned early anaphase spindle (arrow in e). The dashed line delineates the

borders of the cell. The arrow in the middle panel (DAPI channel) shows a misplaced chromosome. Bars: (a, b, c, c′, d) 10 μm; (e) 5 μm.

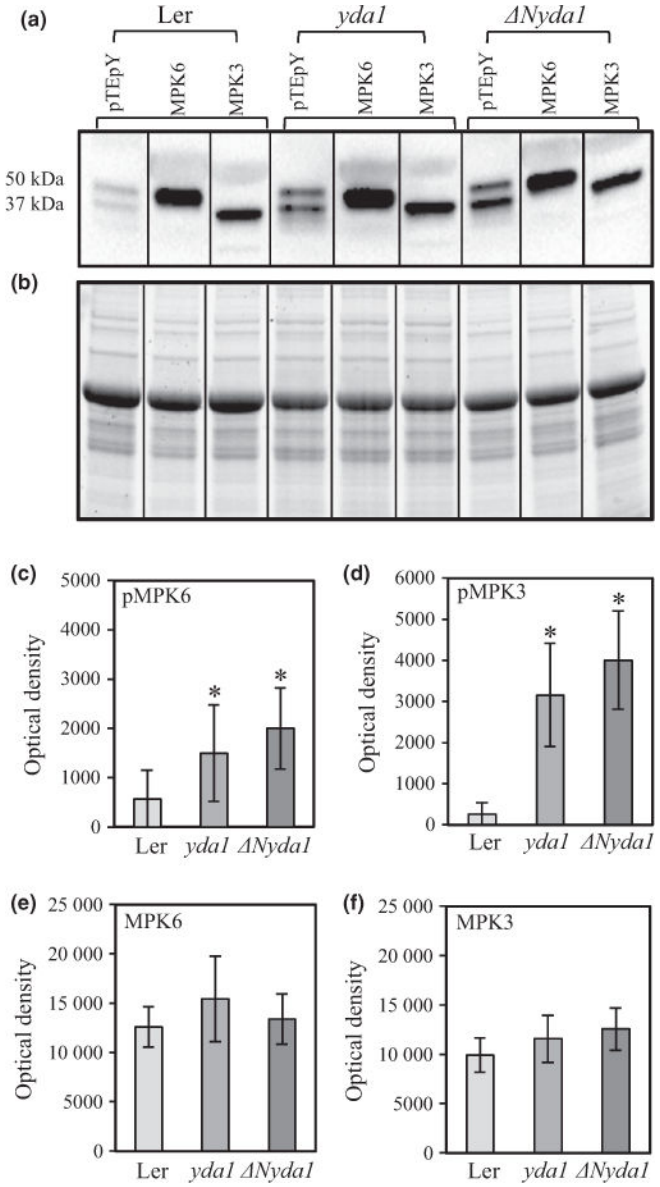

Fig. 10.

Quantitative analysis of protein levels and phosphorylation of MPK3 and MPK6 in extracts from Landsberg erecta (Ler), *yda1* and Δ*Nyda1* Arabidopsis plants. (a, b) Representative western blots from Ler, *yda1* and Δ*Nyda1* probed with antibodies against the pTEpY motif, MPK6 and MPK3 (a) with respective loading control using stain-free gel (b). Vertical bars in (a) and (b) denote that the blot is assembled from strips as described in the Materials and Methods section. (c–f) Graphic depiction of band optical densities (mean ± SD; averaged from three biological repeats) from three independent western blots. Band optical densities correspond to pMPK6(c), pMPK3 (d), total MPK6(e) and total MPK3 (f). *, $P<0.05$

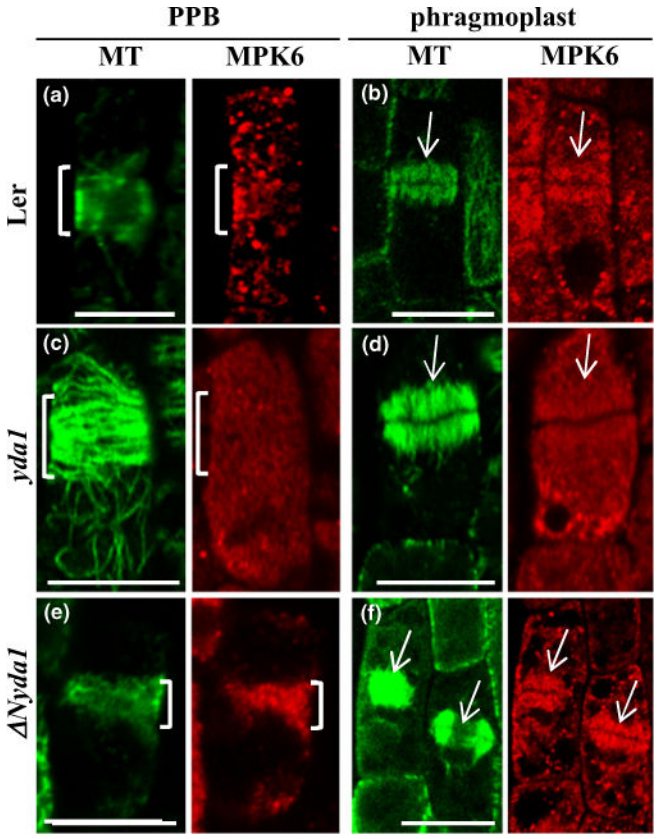

Fig. 11.

Immunofluorescent co-localization of MPK6 and microtubules in preprophase and cytokinetic cells of Arabidopsis Landsberg erecta (Ler), *yda1* and Δ*Nyda1*. (a) Spotlike accumulation of MPK6 fluorescence in the vicinity of the preprophase band (PPB) in a Ler epidermal preprophase cell (brackets in both panels). (b) Accumulation of MPK6 signal within a phragmoplast of a Ler cytokinetic cell (arrows). (c) Absence of MPK6 localization from the PPB (brackets) of a *yda1* epidermal preprophase cell. (d) The phragmoplast of a yda1 cytokinetic cell is devoid of MPK6 immunofluorescence (arrows). (e) Spot-like decoration of PPB (brackets) with MPK6 in a Δ*Nyda1* root epidermal preprophase cell. (f) MPK6 labeling of two phragmoplasts in epidermal cytokinetic cells of Δ*Nyda1*. Bars, 10 μm.

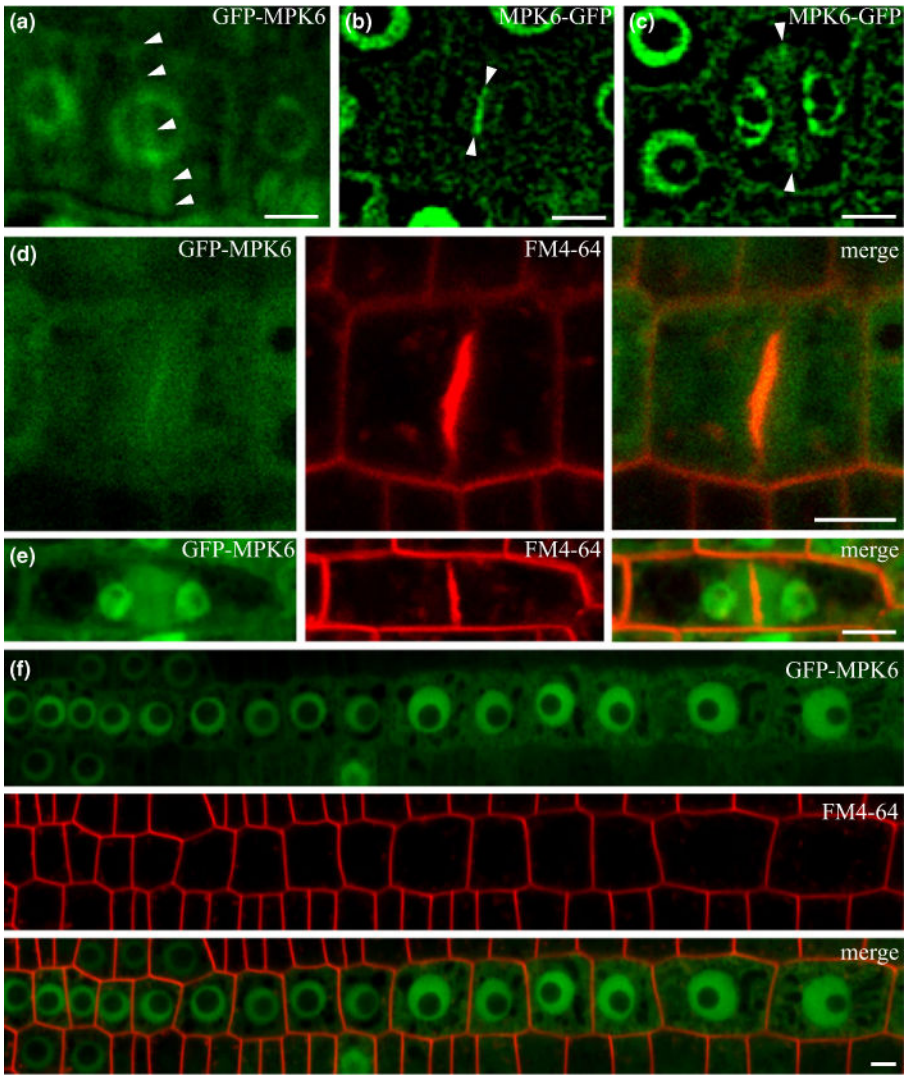

Fig. 12.

Localization of MPK6 in Arabidopsis *mpk6-2* mutants expressing C-and N-terminal GFP fusion of MPK6 under control of *MPK6* promoter. GFP-tagged MPK6 was associated with preprophase band (PPB) (a), early phragmoplast (b), late phragmoplast (c, e), phragmoplast and cell plate (b, d). In interphase root cells (f), MPK6 was localized in nuclei and the cytoplasm. Arrowheads indicate PPB (a) and the middle plane of the phragmoplast (b, c). Live cell imaging of MPK6 in lightsheet microscopy (a) and confocal microscopy (b–f) in cells counterstained with FM4-64. Bars, 5 μm.

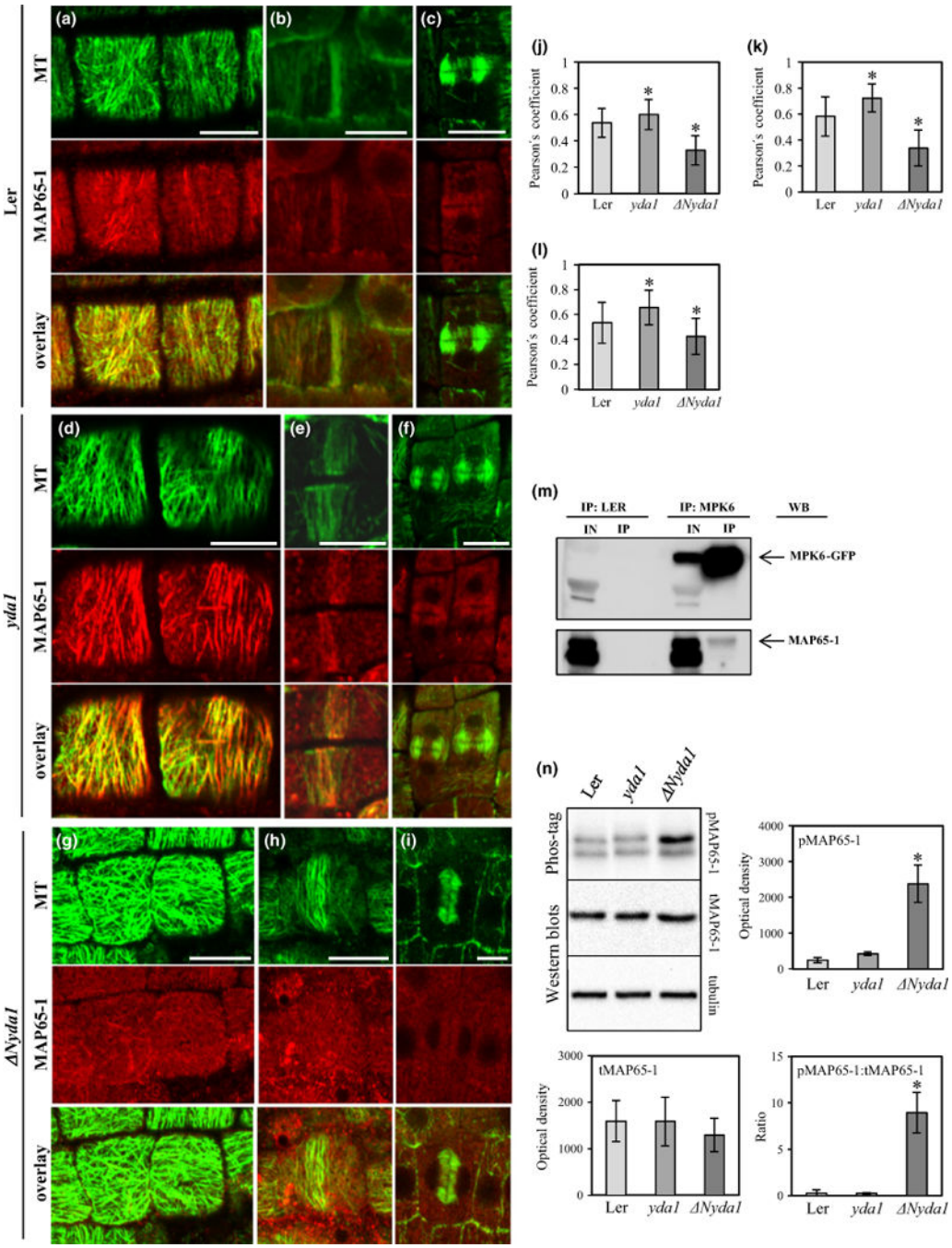

Fig. 13.

Qualitative and quantitative immunofluorescent co-localization of MAP65-1 with microtubules, and abundance and phosphorylation levels of MAP65-1 in Arabidopsis Landsberg erecta (Ler), *yda1* and Δ*Nyda1* plants. (a–c) Co-localization of MAP65-1 with cortical microtubules (a), preprophase bands (PPBs; b) and phragmoplasts (c) in Ler. (d–f) Co-localization of MAP65-1 with cortical microtubules (d), PPBs (e) and phragmoplasts (f) in *yda1*. (g–i) Co-localization of MAP65-1 with cortical microtubules (g), PPBs (h) and phragmoplasts (i) in Δ*Nyda1*. (j–l) Averaged Pearson's coefficients (mean ± SD) from

quantitative MAP65-1/microtubule co-localizations in cortical arrays (j; *N* = 38, *N* = 38, and *N* = 31 for Ler, *yda1* and Δ*Nyda1*, respectively), PPBs (k; *N*= 10, *N*= 21, and *N* = 19 or Ler, *yda1* and Δ*Nyda1*, respectively) and phragmoplasts (l; *N*= 17, *N*= 21, and *N* = 13 for Ler, *yda1* and Δ*Nyda1*, respectively). *, $P<0.05$. (m) GFP-Trap_Aco-immunoprecipitation of MPK6 and MAP65-1. The upper panel shows pulled down MPK6-GFP from the crude extract from plants expressing MPK6-GFP. The bottom panel shows a faint band corresponding to MAP65-1 after western blot probing with anti-MAP65-1 antibody. IN, input; IP, (co)-immunoprecipitated proteins; WB, western blot. (n) Representative Phos-Tag™ (top panel) and western blots of MAP65-1 (middle panel) against tubulin loading control (bottom panel) and graphic depiction (mean ± SD) of phospho-MAP65-1 (pMAP65-1; top panel) total MAP65-1 (tMAP65-1; middle panel) and ratio of pMAP65-1 to tMAP65-1 (bottom panel). *, $P<0.05$. Bars, 10 μm.